INVESTIGATE THE INTERACTIONS BETWEEN SILVER NANOPARTICLES AND SPINACH LEAF BY SURFACE ENHANCED RAMAN SPECTROSCOPIC MAPPING

INVESTIGATE THE INTERACTIONS BETWEEN SILVER NANOPARTICLES AND SPINACH LEAF BY SURFACE ENHANCED RAMAN SPECTROSCOPIC MAPPING

A Thesis Presented

by

ZHIYUN ZHANG

Submitted to the Graduate School of the
University of Massachusetts Amherst in partial fulfillment
of the requirements for the degree of

MASTER OF SCIENCE

SEPTEMBER 2016

Food Science

INVESTIGATE THE INTERACTIONS BETWEEN SILVER NANOPARTICLES AND SPINACH LEAF BY SURFACE ENHANCED RAMAN SPECTROSCOPIC MAPPING

A Thesis Presented

by

ZHIYUN ZHANG

Approved as to style and content by:

_____

Lili He, Chair

_____

Amanda Kinchla, Member

_____

Baoshan Xing, Member

_____

Eric Decker, Department Head

Food Science

DEDICATION

To my parents, thank you very much for your love and support for my study and life.

ACKNOWLEDGMENTS

I would like to thank my advisor, Professor Lili He, for her guidance and oversight in this research project and the support throughout my degree. She helped me develop the independent study, critical thinking and important technical skills. I would also like to extend my gratitude to my committee members, Professors Amanda Kinchla and Professor Baoshan Xing. I am grateful for their helpful recommendations and valuable time.

A special thanks to the entire Prof. Lili He's group. Thanks for the help from all the members past and present in the group. The friendship, collaboration, encouragement and advice have been my good memory. Thanks also goes to Louis Raboin and Dr. Alexander Ribbe from polymer science department, for their technical assistance with the TEM and SEM images. This work is supported by U.S. Department of Agriculture, National Institute of Food and Agriculture (USDA 2015-67017-23070).

ABSTRACT

INVESTIGATE THE INTERACTIONS BETWEEN SILVER NANOPARTICLES AND SPINACH LEAF BY SURFACE ENHANCED RAMAN SPECTROSCOPIC MAPPING

SEPTEMBER 2016

ZHIYUN ZHANG, B.S., SHANGHAI NORMAL UNIVERSITY

M.S., UNIVERSITY OF MASSACHUSETTS AMHERST

Directed by: Professor Lili He

Owing to their increasing application and potential toxicity, engineered nanoparticles (ENPs) have been considered as a potential agricultural contaminant that may pose unknown risk to human beings. However, many techniques require invasive and complicated sample preparation procedures to detect and characterize engineered nanomaterials in complex matrices. In the first part of this thesis, we present a non-destructive and label-free approach based on surface enhanced Raman spectroscopic (SERS) mapping technique to qualitatively detect and characterize gold nanoparticles (AuNPs), on and in spinach leaves in situ. We were able to detect the clearly enhanced signals from AuNPs at 15 to 125 nm on and in spinach leaves. Peak characterizations revealed the aggregation status of Au NPs and their interactions with plant biomolecules, such as chlorophylls and carotenoids. This developed approach will open a new analytical platform for various researches on studying ENPs' adhesion and accumulation.

The second part focuses on investigating the interaction between AgNPs and plant leaves using surface enhanced Raman spectroscopy. AgNPs of different surface coating

(citrate, CIT and polyvinylpyrrolidone, PVP) and size (40 and 100 nm), were deposited onto spinach leaves. SERS signals produced from all kinds of AgNPs exhibited a unique C-S stretching peak at 650-680 cm^{-1}. *In vitro* study indicates this peak may originate from the interaction between AgNPs and cysteine-like compounds based on the peak pattern recognition. The interaction between AgNPs and the cysteine-like compounds happened as soon as 0.5 h after AgNPs exposure. The *in situ* replacement of the CIT with the cysteine-like compounds on the AgNP surfaces was faster compared to that of the PVP. Based on the mapping of the highest C-S peak, we observed the CIT-AgNPs penetrated faster in spinach leaves than the PVP-AgNPs, although the penetration profile for both of them is similar after 48 h ($P < 0.05$). The 40 nm CIT-AgNPs was able to penetrate deeper (to the depth of 183 ± 38 μm) than the 100 nm CIT-AgNPs (to the depth of 90 ± 51 μm) after 48 h. The results obtained here demonstrate the size of AgNPs is the main factor that affects the penetration depth, and the surface coating mainly affects the initial speed of interaction and penetration. This study helps us to better understand the distribution and biotransformation of AgNPs in plants.

In the third part, the removal efficiency of postharvest washing on AgNPs that had accumulated on fresh produce was evaluated. Ten μL commercially available 40 nm citrate coated AgNPs (0.4 mg L^{-1}) were dropped to a (1×1 cm^2) spot on spinach leaves, followed by washing with deionized water (DI water), Tsunami® 100 (80 mg L^{-1}) or Clorox® bleach (200 mg L^{-1}). Then, AgNPs removal efficiency of the three treatments was evaluated by surface enhanced Raman spectroscopy (SERS), scanning electron microscopy (SEM)-energy dispersive spectrometer (EDS), and inductively coupled plasma mass spectrometry (ICP-MS). ICP-MS results showed that deionized water removed statistically insignificant

amounts of total Ag, whereas Tsunami® 100 and Clorox® bleach yielded 21% and 10% decreases in total Ag, respectively ($P < 0.05$). The increased removal efficiency resulted from Ag NPs dissolution and Ag^+ release upon contact with the oxidizing agents in Tsunami® 100 (peroxyacetic acid, hydrogen peroxide) and Clorox® bleach (sodium hypochlorite). According to the SERS results, the deionized water and Tsunami® 100 treatments removed nonsignificant amounts of AgNPs. Clorox® bleach decreased Ag NPs by more than 90% ($P < 0.05$), however, SEM-EDS images revealed the formation of large silver chloride (AgCl) crystals (162 ± 51 nm) on the leaf, which explained low total Ag removal from ICP-MS. This study indicates current factory washing methods for fresh produce may not be effective in reducing AgNPs (by water and Tsunami® 100) and total Ag (by all three means). This highlights the necessity to develop an efficient washing method for NP removal from food surfaces in the future.

TABLE OF CONTENTS

Page

ACKNOWLEDGMENTS v

ABSTRACT..... vi

LIST OF TABLES..... xiii

LIST OF FIGURES xiv

LIST OF ABBREVIATIONS..... xvii

CHAPTER

1. INTRODUCTION 1

2. LITERATURE REVIEW 5

2.1 Introduction to Silver Nanoparticles.....5

2.2 Terrestrial Trophic Transfer of Engineered Nanoparticles.....6

2.3 Toxicity of Silver Nanoparticles to Mammalian Cells 7

2.4 Current Analytical Techniques for Study of AgNPs in Edible Plants and Their Challenges 8

2.4.1 Microscopy and Microscopy-related Techniques.....8

2.4.2 Chromatography and Related Techniques 9

2.4.3 Mass Spectrometry.....9

2.4.4 Spectroscopic and Related Techniques.....10

2.5 Surface Enhanced Raman spectroscopy 10

2.5.1 Introduction to Surface Enhanced Raman Spectroscopy.....10

2.5.2 Current Application of SERS in Agricultural Science 12

3. MAPPING GOLD NANOPARTICLES ON AND IN EDIBLE LEAVES *IN SITU* USING SURFACE ENHANCED RAMAN SPECTROSCOPY.....14

3.1 Introduction.....14

3.2 Materials and Methods.....17

3.2.1 Materials 17

3.2.2 Fabrication and Characterization of Au NPs 17

3.2.3 Preparation for *in situ* Study of Au NPs Adsorbed on Spinach Leaf Surfaces 18

3.2.4 Preparation for *in situ* study of Au NPs Penetrated into Spinach Leaves 18

3.2.5 Raman Instrumentation and Data Aanalysis.....18

3.2.6 Transmission Electron Microscopy Characterization of Au NPs in Spinach.....19

3.3 Results and Discussion 19

3.3.1 In situ Detection and Characterization of Au NPs on Spinach Leaves 19

3.3.2 Raman mapping of Au NPs of Various Sizes on Spinach Leaves 26

3.3.3 *In situ* Detection and Characterization of Au NPs in Spinach Leaves 28

3.3.4 Raman Mapping of Au NPs of Various Sizes in Spinach Leaves 31

3.3.5 Validation of the SERS Mapping Using TEM-EDS.....35

3.4 Conclusion 36
4. EVALUATION OF POSTHARVEST WASHING ON AGNPS REMOVAL FROM SPINACH LEAVES.....38
4.1 Introduction.....38
4.2 Materials and Methods.....40
4.2.1 Materials 40
4.2.2 Preparation for *in situ* Study of AgNPs Penetration on Spinach.....41
4.2.3 Determination of The SERS Characteristic Signals of Various Pesticides on Gold Coated Glass Slide 41
4.2.4 Raman Instrumentation and Data Analysis.....41
4.3 Results and Discussion 43
4.3.1 Interactions of Biomolecules and AgNPs in Spinach Leaf.....43
4.3.2 Size Effect on Biotransformation and Penetration Behavior.....47
4.3.3 Surface Coating Effect on Biotransformation and Penetration Behavior.....53
4.4 Conclusion 54
5. EVALUATION OF POSTHARVEST WASHING ON AGNPS REMOVAL FROM SPINACH LEAVES.....55
5.1 Introduction.....55
5.2 Materials and Methods.....57
5.2.1 Spinach Samples and AgNPs.....57
5.2.2 Washing Sanitizer and Washing Conditions.....58

5.2.3 Recovery of Surface AgNPs Residue for SERS Measurement 59
5.2.4 Scanning Electron Microscopy (SEM) 59
5.2.5 Inductively Coupled Plasma-Mass Spectrometry (ICP-MS).....60
5.2.6 Statistical Analysis.....60
5.3 Results.....60
5.3.1 Effectiveness of SERS-Based Method to Detect and Identify AgNPs.....60
5.3.2 Standard Curve Establishment for AgNPs Quantification.....62
5.3.3 Quantification of AgNPs on Leaves after Washing Using SERS.....64
5.3.4 Evaluation the Total Ag Removal and Ag species after Washing Using ICP-MS and SEM-EDS.....65
6. CONCLUDING REMARKS.....72
BIBLIOGRAPHY.....74

LIST OF TABLES

Table Page

5. 1 Silver amounts on treated and washed spinach using ICP-MS and SERS 65

LIST OF FIGURES

Figure Page

3. 1 Bright light scattering images, Raman images, and Raman spectra of spinach leaf with and without 35 nm Au NPs. (a) and (b), bright light scattering image and Raman image of spinach leaf without Au NPs. (c) and (d), bright light scattering image and Raman image of spinach leaf with Au NPs. (e)-(h), Raman spectra of selected spots on Raman images. The step size of the mapping is 10 μm and one image contains 100 scanning spots. 23

3. 2 SERS spectra of pigments (chlorophylls and carotenoids) extracted from spinach leaves mixed with Au NPs of different sizes (15-125 nm). The detailed extraction was adapted by a published protocol78</sup> as follows. 100 μL extracted solu*t*ions (500 mg L^{-1}) were mixed with 100 μL Au NPs at 50 mg L^{-1} for 30 min, then the Au NPs were deposited on a gold coated glass slide for Raman measurement. Compared with control (just pigments without Au NPs), all the Au NPs show enhanced signals. The SERS spectra obtained was found similar to the *in situ* SERS spectra of Au NPs on and in spinach leaves, indicating the Au NPs were interacted with plant pigments on and in spinach leaves. 15 nm Au NPs shows the least enhancement, while the 125 nm Au NPs show the most enhancements. The similar size dependent SERS enhancement was also reported in other study.[2] 24

3. 3 Estimation of false positive (2%) and false negative (5%) of the mapping method with the baseline set at 200 counts based on the 1525 cm^{-1} peak. (a) 2D Raman mapping of spinach leaf without Au NPs. Two out of 100 points had higher than 200 counts, (b) 2D Raman mapping of the spinach leaf with Au NPs. Five out of 100 points contain characteristic peaks of Au NPs but had lower than 200 counts, (c) representative spectrum of the false positive signal, (d), representative spectrum of the false negative signal. 25

3. 4 SERS spectrum of Au NPs aggregates dried on a gold coated slide. A broad peak over 1000-1700 cm^{-1} was observed, which is similar to the *in situ* spectra observed from Au NPs on and in spinach leaves. The intensity of the signals on a gold slide was higher than that on and in spinach leaves because of the better reflectivity of the gold slide. 26

3. 5 Raman images of spinach leaves with Au NPs of different sizes (15-125 nm) and concentrations (50 and 5 mg L^{-1}). (a), spinach leaves without Au NPs. (b1)-(e1), spinach leaves with 50 mg L^{-1} Au NPs of different sizes. (b2)-(e2), spinach leaves with 5 mg L^{-1} Au NPs of different sizes. Step size is 40 μm and one image contains 360 scanning points. 28

3. 6 Raman images and selected SERS spectra of Au NPs in spinach leaves. (a)-(c), Raman images in different depth profile (0, 10, and 20 μm). (d)-(f) are SERS spectra at the same spot in different depth profile (0, 10, and 20 μm). (g), Raman depth image of spinach without Au NPs. (h)-(j) are Raman depth images of spinach with Au NPs. For surface mapping (a-c), the step size is 10 μm and each image contains 100 spots. For depth mapping (h-k), the step size in X direction is 10 μm and in Z direction is 10 μm, and each image contains 150 spots..... 30

3. 7 SERS spectra of different spots in spinach leaves at 20 μm depth *in situ*. They show different patterns combining the characteristic peaks of carotenoids and chlorophylls, as well as the sulfur peaks, which demonstrate the strong interactions with plant pigments and sulfur containing compounds. 31

3. 8 Raman images of Au NPs with different sizes (15-125 nm) and concentrations (50 and 200 mg L^{-1}) in spinach leaves. (a), spinach leaves without Au NPs. (b1)-(e1), spinach leaves with 50 mg L^{-1} Au NPs of different sizes. (b2)-(e2), spinach leaves with 200 mg L^{-1} Au NPs of different sizes. The step size in X direction is 10 μm and in Z direction is 10 μm, and each image contains 150 spots..... 32

3. 9 Optical images of representative selected areas for studying stomata and cuticle penetration, and SERS mapping of penetration depth profiles of 35 nm Au NPs through randomly picked stomata and cuticle on spinach leaf surfaces. Both of these two penetration pathways show variations in term of penetration depth, and there is no statistical difference between them. Stomata may allow more Au NPs to penetrate in some cases, as indicated by intense signals observed in the depth profile. 33

3. 10 Optical (a) and 2D Raman mapping (b) of the cross section of the spinach leaves deposited with 35 nm Au NPs. (c-k) SERS spectra collected from different depths..... 35

3. 11 TEM-EDS images of spinach leaves treated with 35 nm Au NPs (200 mg L^{-1}). Chloroplast (Chl) and Cell wall (CW)..... 36

4. 1 (a) SERS spectra of 40 nm CIT-AgNPs in different position of spinach leaf; (b) SERS spectra of 40 nm CIT-AgNPs in different depth (depth: 0 to 190 μm) of spinach leaf. 43

4. 2 SERS spectra of the interactions between different biomolecules and (a) 40 nm CIT-AgNPs, (b) 100 nm CIT-AgNPs and (c) 40 nm PVP-AgNPs. 45

4. 3 (a), (b), (c) *In situ* SERS spectra of 40 nm CIT-AgNPs, 100 nm CIT-AgNPs, 40 nm PVP-AgNPs in spinach leaf following different exposure time; (d), (e), (f) Second derivative Raman spectra of the C-S stretching peak of cysteine from 40 nm CIT-AgNPs, 100 nm CIT-AgNPs, 40 nm PVP-AgNPs in spinach leaf following different exposure time. 47

4. 4 SERS spectra of the interactions between cysteine and (a) 40 nm CIT-AgNPs, (b) 100 nm CIT-AgNPs and (c) 40 nm PVP-AgNPs following different time (0.5 and 48 h)..... 48

4. 5 Principal component analysis (PCA) plot of (a) 40 nm CIT- and 100 nm CIT-AgNPs in spinach leaf with different time (0.5 and 48 h), (b) 40 nm CIT- and PVP-AgNP in spinach leaf with different time (0.5 and 48 h)..... 49

4. 6 2D SERS depth mapping images of (a) 40 nm CIT-AgNPs, (b) 100 nm CIT-AgNPs, (c) 40 nm PVP-AgNPs penetration following different exposure time based on the highest C-S stretching peaks; (d), (e) Comparison of penetration depth of AgNPs with different sizes (40 and 100 nm) and surface coatings (CIT and PVP) in spinach following different exposure time. Results are expressed as mean value standard deviation (n=3). Different letters represent a significant difference ($P<0.05$)..... 50

5. 1 (a) AgNPs collection process from a spinach leaf; (b) Sample mixed with 100 mg L^{-1} 4-Mercaptobenzoic acid; (c) Detection process with the DXR Raman spectrometer; (d) schematic drawing for the detection of AgNPs. 61

5. 2 SERS spectra of deionized water (negative control), $AgNO_3$, AgCl, Ag NPs with 100 mg/L 4-Mercaptobenzoic acid..... 62

5. 3 (a) SERS spectra of different concentrations of 40 nm AgNPs with 100 mg L^{-1} 4-Mercaptobenzoic acid; (b) second derivative Raman spectra of the characteristic peak of 4-Mercaptobenzoic acid at 1078 cm^{-1}; (c, d, e) the linear relationship between Raman intensity and AgNPs concentration; The error bars represent the standard errors of three parallel SERS measurements. 64

5. 4 (a) SERS spectra of different washing treatments on 40 nm AgNPs (40×10^{-5} mg) contaminated spinach leaves; (b) second derivative Raman spectra of the characteristic peak of 4-Mercaptobenzoic acid at 1078 cm^{-1}. 65

5. 5 SEM images of spinach leaf surfaces treated with 4×10^{-4} mg AgNPs: (a) raw spinach leaf without AgNPs; (b) AgNPs treated spinach leaves; (c) deionized water washed; (d) 80 mg L^{-1} Tsunami® 100 treated; (e) 200 mg L^{-1} Clorox® bleach solution treated. 66

5. 6 The size distribution of residual particles on spinach after postharvest washing. ... 67

5. 7 EDS analysis of spinach leaf surfaces treated with 4×10^{-4} mg AgNPs: (a) raw spinach leaf without AgNPs; (b) AgNPs treated spinach leaves; (c) deionized water washed; (d) 80 mg L^{-1} Tsunami® 100 treated; (e) 200 mg L^{-1} Clorox® bleach solution treated. 68

LIST OF ABBREVIATIONS

SERS – Surface enhanced Raman Spectroscopy

AuNPs – Gold Nanoparticles

AgNPs – Silver Nanoparticles

CuNPs – Copper Nanoparticles

ENPs – Engineered Nanoparticles

EPA – Environmental Protection Agency

SEM – Scanning Electron Microscopy

TEM – Transmission Electron Microscopy

EDS – Coupled Energy Dispersive X-Ray Spectroscopy

ICP-MS – Inductively Coupled Plasma Mass Spectrometry

ICP-OES – Inductively Coupled Plasma Optical Emission Spectrometry

μXRF – Micro X-Ray Fluorescence

XAS – X-Ray Absorption Spectroscopy

LSPR – Localized Surface Plasmon Resonance

ROS – Reactive Oxygen Species

SEC – Size Exclusion Chromatography

CE – Capillary Electrophoresis

HDC – Hydrodynamic Chromatography

FFF – Field-Flow-Fractionation

DLS – Dynamic Light-Scattering

UV-Vis – UV–Vis Spectroscopy

FTIR – Fourier Transformation Infrared Spectroscopy

NMR – Nuclear Magnetic Resonance

Chl – Chloroplast

CW – Cell Wall

CIT – Citrate

PVP – Polyvinylprrolidone

Cys – Cysteine

GSH – Glutathione

γ-ECS – γ-glutamylcysteine

GS – Glutathione Synthase

GSSG – Glutathione Disulfide

GR – Glutathione Reductase

PCs – Phytochelatins

4-MBA – 4-Mercaptobenzoic acid

ANOVA – Analysis of Variance

PCA – Principal Component Analysis

CHAPTER 1

INTRODUCTION

Silver nanoparticles (AgNPs) has been known for its unique antimicrobial and insecticidal properties over 100 years.[1] For example, numerous studies on the toxicity of AgNPs to different bacterial species, including *E. coli*, *Bacillus subtilis*, *Nitrosomonas europaea*, *Pseudomonas fluorescens*, and *Pseudomonas aeruginosa* have been performed in detail.[2] In recent years, there has been increased interest in the use of inorganic pesticides, such as those containing AgNPs. The manufacturers of these products anticipate that these new pesticides will have greater efficacy in the field, which will subsequently decrease pesticide releases through environmental or "spray" drift and storm water runoff.[3] Currently in the US, approximately 110 AgNPs-containing products had been registered as pesticides by the EPA and several patent applications for AgNPs-based fungicides had been filed.[4,5] The global production of AgNPs was estimated at 500 tons per year and significant increases are anticipated in the future.[6] However, the widely use of AgNPs-based pesticides may increase the likelihood of human exposure, for example, unintentional consumption of AgNPs contaminated crop plants, which may pose risks to human beings. So far, the toxicity of AgNPs to human cells, such as oxidative stress, genotoxicity, and apoptosis have been demonstrated by several studies. For example, after 24 h treatment, 5-10 nm AgNPs with concentration from 0.05 mg L^{-1} to 20 mg L^{-1} could result in oxidative stress, DNA damage, cell cycle arrest and apoptosis in human jurkat cells.[7] Therefore, detecting AgNPs and understanding their bio-fates in plants is a prerequisite.

Up to date, there are a lot of techniques have been used to study AgNPs in edible plants. For qualitative analysis, electron microscopy techniques, including scanning electron microscopy (SEM) and transmission electron microscopy (TEM) coupled energy dispersive X-ray spectroscopy (EDS), are the most common techniques that be used to image the size and morphology of AgNPs in plants. However, in addition to complex sample preparation procedures, the major limitation of TEM/SEM-EDS is that both of them have to be operated under vacuum conditions. In other words, biological samples must be fully dehydrated and cryo-fixed/embedded before being introduced to the sample chamber, which usually results in sample alteration and dehydration artifacts.[8] For quantitative analysis, several elemental quantification techniques, especially inductively coupled plasmamass spectrometry (ICP-MS) or inductively coupled plasma optical emission spectrometry (ICP-OES), are the normal techniques to measure total Ag concentration, but limited information regarding Ag speciation can be reflected.[9] Currently, more advanced techniques, such as Micro X-ray fluorescence (μXRF) and X-ray absorption spectroscopy (XAS) have also been used to study AgNPs in plants. However, access to these advanced techniques is limited. More importantly, complicated sample preparation procedures make them impossible to study AgNPs in plants *in situ* and real time. As a result, a technique that can be used to *in situ* and real time detect and characterize AgNPs in plants is urgently needed.

Surface enhanced Raman spectroscopy (SERS) is an advanced technique that involves both Raman spectroscopy and nanoscale noble metal substrates. This new analytical platform possesses the advantages of Raman spectroscopy, such as small sample size, minimal sample preparation, rapid spectrum collection, and characteristic fingerprint

for specific analytes.[9] More importantly, two inherent drawbacks of Raman spectroscopy, weak intensity and fluorescence interference are resolved.[10] This is because the excitation of localized surface plasmon resonance (LSPR) on nanoscale-roughed surface can generate a large electromagnetic field which increases the Raman cross section from the molecules adsorbed to noble metal nanostructures.[11] In addition, through selecting less energetic excitation or detecting analytes that are close to the SERS-active metal surface with a quenching effect, low background autofluorescence can be achieved.[10] Due to these advantages, SERS has been applied in many areas, including chemistry,[12,13] molecular biology,[14–16] medicine,[17,18] food analysis[19–21] and environmental contaminants detection.[22,23]

Herein, we focused on two significant knowledge gaps in the study of AgNPs contaminants in plants, (1) *in situ* and real time detect AgNPs in plants; (2) characterize the interactions between AgNPs and plants.

To fill these two critical knowledge gaps, the following objectives were pursued:

Objective 1: Establish SERS mapping method to detect and characterize gold nanoparticles (AuNPs) on and in spinach leaf. The objective of this experiment is to evaluate the feasibility of SERS mapping to detect AuNPs and investigate the interactions between AuNPs and spinach leaf.

Objective 2: In situ and real time investigate the interaction between AgNPs and spinach leaf using SERS mapping. The objective of this experiment is to investigate the interactions between AgNPs and plant leaves using surface enhanced Raman spectroscopy.

Objective 3: Evaluate the postharvest washing on AgNPs removal from spinach leaves. The objective of this experiment is to determine whether postharvest washing can effectively remove AgNPs that had accumulated on fresh produce.

The innovation of this study relies on taking advantage of the unique property of SERS to detect AgNPs and characterize the signals from the biomolecules adsorbed on those AgNPs. Through analyzing the SERS spectrum of interactions between AgNPs and biomolecules, the physical and molecular mechanisms that allow AgNPs to attach onto and internalize into spinach leaf can be understood. With the mapping technique, quantification of AgNPs and non-invasively study of their distribution on and in plant leaf can also be achieved. To the best of our knowledge, this is the first study to use SERS mapping to detect AgNPs contaminants and characterize the AgNPs-biomolecules interactions in edible plant leaves.

CHAPTER 2

LITERATURE REVIEW

2.1 Introduction to Silver Nanoparticles

Nanoparticles, by definition, are structures that possess one or more external dimensions in the range of 1-100 nm and are increasingly used in a wide spectrum of technical applications and consumer products due to their unique properties. Among all the nanoparticles in consumer products, silver nanoparticle (AgNPs) applications currently have the highest degree of commercialization,[24] which covers from pigments, photographics, wound treatment, conductive/antistatic composites, catalysts, to biocides.[1] The global production of AgNPs was estimated at 500 tons per year and significant increases are anticipated in the future.[6] Although the term "nanotechnology" was first used by Norio Taniguchi in 1974 and emergence of nanotechnology as a field occurred in the 1980s, the synthesis of citrated-stabilized AgNPs has already been reported by M. C. Lea as early as in 1889.[25] In this method, the average diameter of the synthesized AgNPs is between 7 and 9 nm.[26] Due to its unique antimicrobial properties, the primary commercial use of AgNPs was mainly for medical application. In 1897, AgNPs has been manufactured commercially under the name "Collargol".[27] The mean size of AgNPs in Collargol is around 10 nm and its diameter was determined to be in the nanorange in 1907. In the early part of the 20th century, the commercial sale of medicinal AgNPs, known under different names, such as Collargol, Argyrol, and Protargol became widespread. All these AgNPs contained products were sold as over-the-counter medications and applied for various diseases treatment, such as syphilis and other bacterial infections.[28]

Apart from these medical applications, a lot of biocidal products that contained AgNPs were developed and registered in the United States. Algaedyn is the first biocidal silver product registered in the United States under the Federal Insecticide, Fungicide, and Rodenticide Act (FIFRA) in 1954, and is still used today as an algicide in residential swimming pools.[1] Since the establishment of US-EPA in 1970, the frequency of EPA-registered silver products has been steadily increasing. EPA-registered AgNPs containing-products can be divided into three categories; (a) AgNPs biocidal additives, (b) Ag-impregnated water filters, and (c) Ag algicides and disinfectants.[1] In recent years, there has been increased interest in the use of inorganic pesticides, such as those containing AgNPs. For example, Kim et al. tested the effectiveness of AgNPs against powdery mildew on *Sphaerotheca pannosa var. rosae* in the field.[29] They found that a decline in mildew infestation of 95% a week after the application of 15 g AgNPs ha^{-1}. Compared with the application rates of conventional fungicides against powdery mildew (range from 105 g to 6 kg ha^{-1}), AgNPs could be applied in lower amounts, achieving the same effect. Similar result was also reported by Alavi and Dehpour,[30] who showed a higher efficiency of a commercial Ag NM product (Nanocid L2000) compared to a conventional fungicide. Both the researchers and manufacturers anticipate that these new pesticides will have greater efficacy in the field, which will subsequently decrease pesticide releases through environmental or "spray" drift and storm water runoff.[3]

2.2 Terrestrial Trophic Transfer of Engineered Nanoparticles

With the increasingly use of AgNPs in agricultural areas, there is an urgent need to understand the trophic transfer of AgNPs within terrestrial food webs when assessing AgNPs fate, disposition and effects. However, limited studies have been conducted and

only three reports regarding the terrestrial trophic transfer and biomagnification of ENMs have been published. Judy et al. reported the trophic transfer of AuNPs from tobacco [*Nicotiana xanthi*] to tobacco hornworm [*Manduca sexta*]. Their working demonstrated that bioaccumulation factors (BAFs) of 6.2, 11.6, and 9.6 for tobacco hornworm consuming 5, 10 and 15 nm AuNPs contaminated leaves of tobacco [*Nicotiana xanthi*].[31] In another study conducted by the same group, comparatively smaller BAF (0.16) for caterpillars consuming AuNPs contaminated tomato [*Lycopersicon esculentum* L.] leaves was observed.[32] It should be noted here, although no symptoms of AuNPs toxicity in the hornworms were observed, their findings indicate the potential trophic exposure and biomagnification. Therefore, considerable work in this critical area is urgently needed to ensure food safety.

2.3 Toxicity of Silver Nanoparticles to Mammalian Cells

As shown in Table 1 and Table 2, there are a lot of in vitro and in vivo studies demonstrated the potential toxicity of AgNPs to cells derived from a variety of organs. The toxicity of AgNPs likely results from two mechanisms, reactive oxygen species (ROS) generation and oxidative stress.[33] When ROS exceed the capacity of the anti-oxidant defense mechanism, oxidant stress normally occurs. Both ROS and oxidative stress would elicit some physiologic and cellular events, such as stress, inflammation, DNA damage and apoptosis.[34,35] The concentrations of AgNPs used in these studies were range from 1 to 200 μg mL^{-1}, and 5-50 μg mL^{-1} is the most common tested range.[24] It should be noted that AgNPs are toxicity to human cells even at non-cytotoxic doses. For example, Kawata et al. showed that non-cytotoxic doses (<0.5 μg/mL) of AgNPs induced the expression of genes related with cell cycle progression and apoptosis in human hepatoma cells (HepG2).[36]

Greulich et al. also showed that non-cytotoxic doses of AgNPs could result in toxicity in human mesenchymal stem cells.[37]

2.4 Current Analytical Techniques for Study of AgNPs in Edible Plants and Their Challenges

A wide range of techniques are current available for nanoparticles detection and characterization in plants. A brief summary of mainly used techniques are described below.

2.4.1 Microscopy and Microscopy-related Techniques

Microscopy-based techniques include confocal microscopy as well as electron and scanning probe microscopy. Among them, the most popular tools for the visualization of ENPs are transmission electron microscopy (TEM) and scanning electron microscopy (SEM).[8] Resolutions down to the sub-nanometer range can be achieved though using these techniques. In TEM, electrons are transmitted through samples to obtain an image, indicating the samples have to be very thin; In SEM, scattered electrons are detected at the sample interface for imaging. Currently, some analytical tools are coupled to electron microscopes for additional elemental composition analysis, which are known as analytical electron microscopy. Energy dispersive X-ray spectroscopy (EDS) is normally combined with SEM and TEM for a clear determination of the composition of elements. However, for these conventional electron microscopes, all of them have to be performed under vacuum conditions, indicating all tested samples must experience complex sample preparation (dehydration, cryo-fixation or embedding), which may lead to sample alteration and dehydration artifacts.[38]

2.4.2 Chromatography and Related Techniques

Techniques associated to chromatography can be used to separate nanoparticles in samples. Size exclusion chromatography (SEC), capillary electrophoresis (CE) and hydrodynamic chromatography (HDC) are the most common techniques in this field. These techniques are normally considered as rapid, sensitive (detector dependent) and non-destructive. By attaching traditional analytical tools (such as ICP-MS/OES) as detectors to size separation techniques, quantification of different nanoparticles in food, water, biota and soil can be achieved. However, although a range of solvents are compatible for some chromatographic tools, most samples usually cannot be run in their original media, which may cause sample alteration and sample solvent interaction.

2.4.3 Mass Spectrometry

Mass spectrometers normally consist of an ion source, a mass analyzer and a detector system. In the case of inductively coupled plasma mass spectrometry (ICP-MS), inductively coupled plasma (ICP) sources are mainly used for metal analysis. Currently, a combination of field-flow-fractionation (FFF) and ICP-MS gains more attention.[8] This is because FFF-ICP-MS allows the quantitative and elemental analysis of particles with different size fractions. Even though the development of FFF-ICP-MS is promising for nanoparticle analysis, it still owes some unevaded limitations. For example, ICP based methods require digestion of total Ag into Ag ions, therefore the information from ICP cannot reflect as it is from real NPs *in situ*. In addition, when there are chloride ions (Cl^-) present, AgCl particles will form. Electron microscopes cannot differentiate between AgNPs and AgCl NPs. Even coupled with energy dispersion spectroscopy (EDS) which can help identify the elemental composition, its mineral phase cannot be validated.

2.4.4 Spectroscopic and Related Techniques

A variety of spectroscopic methods have been available for nanoparticle analysis and characterization, including dynamic light-scattering (DLS), UV–Vis spectroscopy (UV-Vis), Fourier transformation infrared spectroscopy (FTIR), Nuclear magnetic resonance (NMR), X-ray spectroscopy and so on. In recent years, synchrotron X-ray fluorescence microscopy was used for *in situ* mapping and speciation of CeO_2 and ZnO NPs in soil cultivated soybean,[39] and mapping AuNPs in tobacco hornworm caterpillars. However, disadvantages of this technique, include the additional absorption of characteristic X-rays by the sample itself on their path to the detector system, especially for low energy X-rays or where samples are particularly dense or large (exceeding a few hundred micrometres), absorption effects can be severe and difficult to correct. In addition, access to synchrotron facilities is limited.

2.5 Surface Enhanced Raman spectroscopy

2.5.1 Introduction to Surface Enhanced Raman Spectroscopy

Raman spectroscopy is one branch of vibrational spectroscopy that can be used to study a very wide range of sample. The phenomenon of Raman scattering was first reported by Raman and Krishna in 1928.[40] When monochromatic light encounters a sample, photons are scattered from the sample. Among these scattered photons, most of them are scattered elastically, indicating the energy state of the scattered photons return back to the same state as the incident photon, which is referred as Rayleigh scattering. Rayleigh scattering can be considered as a short lived distortion of electron cloud caused by the oscillating electric field of the light. However, the electron cloud of the molecule is also influenced by molecular vibrations, and it is possible for the optical and vibrational oscillations to

interact, leading to Raman scattering. Contrary to Rayleigh scattering, Raman scattering is a comparatively weak process since only one in 10^6 to 10^8 photons have a frequency different from the incident photons. There are two types of Raman scattering: Stokes and anti-Stokes, which depends on the initial molecular state. Molecules originally in the ground vibrational state result in Stokes Raman scattering while molecules originally in vibrational excited state result in anti-Stokes Raman scattering. The shift in energy reflects the information about the photon modes in the system.[41]

However, the application of Raman spectroscopy was largely impeded by both fundamental and technical issues, especially weak intensity and fluorescence interference. Until 1974, the discovery of surface enhanced Raman effect overcomes these problems. Jeanmaire and Van Duyne demonstrated that greatly enhanced Raman scattering signal can be achieved when the scatterer is on or near a roughened noble metallic (gold, silver, or copper) substrate. Therefore, surface enhanced Raman spectroscopy can be considered as a combined technique that involves both Raman spectroscopy and nanotechnology.

Although the mechanism of SERS enhancement remains an active research topic, there are two mechanisms of SERS enhancement have been proposed, chemical enhancement and electromagnetic enhancement. As for chemical mechanism, a charge-transfer state between the metal and molecules is created. This mechanism is both site-specific and analyte-dependent, meaning the targeted molecule should be directly adsorbed to the roughed surface to experience the chemical enhancement. Currently, it is generally considered that the chemical mechanism contributes an average enhancement factor of 100. Electromagnetic enhancement is the other generally known mechanism involved in SERS enhancement, which is closely depends on many factors, such as material, size, and shape

of noble metallic substrate. When light with specific wavelength is incident upon the noble metallic substrates, the conduction electrons on noble metallic substrates surface undergo a collective oscillation, generally known as surface plasmon resonance (SPR). The excitation of localized surface plasmon resonance (LSPR) on nanoscale-roughed surfaces can generate a large electromagnetic field, which increases the Raman cross section of adsorbed molecules that are in or near to noble metallic substrates. The average enhance factor of electromagnetic fields normally can reach up to 10^5.

2.5.2 Current Application of SERS in Agricultural Science

Currently, SERS has gradually been used in agricultural science for various purpose. For example, Zeiri reported that colloidal gold and silver could be formed by the spontaneous reduction of metal salts in a variety of plant tissue, including alfalfa seed, green tea leaves, carrots and red cabbage.[42] The formation of gold and silver colloids inside plant tissues can further enable SERS measurements (enhanced Raman signals and fluorescence quenching), which yields specific vibrational signatures for the plant components in the proximity of the colloids. Palanco et al. used silver nanoaggregates and silver island films to *in vivo* detect the chemical constituents, such as cellulose, proteins, and flavonols, of onion layer. Their study shows the capacity of SERS to monitor the location of AgNPs inside the onion layers as well as to identify the complex heterogeneous chemical structure of the onion. In addition, through the pH-sensitive reporter molecule-para mercapto benzoic acid (Pmba) , the pH values inside onion can be measured.[43] Shen et al., for the first time, use SERS mapping to non-destructively image a living plant biocompatible with the help of carbon encapsulated Au-Ag nanoparticles.[44]

Apart from the above applications, there is an increasing trend to use SERS to *in situ* detect pesticide and monitor the pesticide penetration in plants. Hou et al. showed the capacity of SERS to *in situ* detect and discriminate different kinds of pesticides in plants.[45] Yang et al. used SERS mapping to real time and *in situ* monitor the pesticide penetration in edible leaves.[46]

CHAPTER 3

MAPPING GOLD NANOPARTICLES ON AND IN EDIBLE LEAVES *IN SITU* USING SURFACE ENHANCED RAMAN SPECTROSCOPY

3.1 Introduction

In recent years, engineered nanoparticles, such as silver and copper, are increasingly used in agriculture due to their antimicrobial properties. For example, silver nanoparticles (Ag NPs) have been widely used to protect crops against plant pathogens and pests.[5] As of 2010, there had been more than 110 officially registered Ag NPs containing pesticides used for agricultural, environmental, medical, and home purposes in the US.[4] Copper based pesticides, including copper nanoparticles (Cu NPs) have also been used widely as fungicides in vineyards and farms.[1] However, the use of these NPs in agriculture may pose some potential risks. A number of studies show that certain engineered nanoparticles (ENPs) are more toxic to microbes, plants, animal and/or human cells compared to their ionic or bulk counterparts.[47] The increasing prevalence of ENPs within agriculture and food products and their potential toxicity has urged researchers to study how those ENPs could possibly contaminate the environment and bioaccumulate along the food chain, and to evaluate their chemical and biological effect on human health and the environment. However, research on ENPs as emerging contaminants is still a new field.[48,49] Some studies suggested that NPs can accumulate in plants after foliar exposure[50–52] and may be able to translocate from soil to plant tissues.[53–55] The interactions between NPs and plants depend on size and surface charge of NPs,[56,57] and are also plant species-specific.[58,59]

These bioaccumulated NPs can enter into food chains; and can then be transferred to consumers, causing unknown risks to sensitive receptors.[49]

Various techniques have been used for detection and characterization of ENPs *in planta*, such as inductively coupled plasma based methods,[50–52,58] X-ray absorption spectroscopy,[57,59–61] and electron microscopy.[50–52] However, the majority of these techniques require complex digestion and extraction procedures for analyzing NPs from complex samples.[8] Synchrotron X-ray fluorescence microscopy has been used for *in situ* mapping and speciation of CeO_2 in kidney beans[39] and cucumber roots.[62] However, there are certain disadvantages of this technique, including the additional absorption of characteristic X-rays by the sample itself on their path to the detector system, especially for low energy X-rays or where samples are particularly dense or large (exceeding a few hundred micrometers), the absorption effects can be severely influenced.[63] In addition, access to synchrotron facilities is limited. Thus, the development of a rapid and reliable method for the detection and characterization of ENPs in complex matrices is needed.

Surface enhanced Raman spectroscopy (SERS) is a combined technique that involves both Raman spectroscopy and nanotechnology. Noble metals, such as NP Au, Ag, and Cu, can significantly enhance the Raman signals of the molecules that are in close vicinity of metal surfaces. This is because the excitation of localized surface plasmon resonance on noble metal NPs can generate a large electromagnetic field that increases the Raman cross section from molecules that are in close proximity (~10 nm) of a noble metal nanostructure.[11] Due to its improved sensitivity, SERS has been applied for the detection of various chemical and biological targets in many areas, such as medical diagnosis,[64] food[21,65] and environmental safety.[23] In addition, SERS mapping has been applied as an

imaging tool for intracellular studies. For example, Rodríguez-Lorenzo et al. utilized SERS-encoded gold nanostars for intracellular mapping.[66] Ando et al. reported a dynamic SERS imaging method based on Au NPs being applied to study dynamic biological functions in living cells, such as membrane protein diffusion, nuclear entry, and rearrangement of cellular cytoskeleton.[67] Shen et al. also found that SERS can be used as a rapid and non-invasive imaging technique to monitor the distribution of 4-mercapto benzoic acid tagged carbon-encapsulated Au-Ag NPs inside the leaf.[44] To date, however, most of the analytical targets for SERS are chemical and biological compounds.

Herein, we aimed at NPs rather than the chemical and biological targets. The objective is to evaluate the SERS technique for *in situ*, non-destructive and label-free detection of Au NPs on and in spinach leaves after foliar exposure and characterization of the interaction between Au NPs and spinach. The innovation of this study lies in the use of intrinsic enhanced SERS signals from the biomolecules to detect the presence of noble metallic nano-contaminants and determine their final fate in plants. Coupled with mapping technique, this SERS method can spatially image the heterogeneous distribution of NPs on and in spinach leaves *in situ* and non-destructively. Au NPs were chosen as the model NPs to evaluate and demonstrate method feasibility, because they can easily be synthesized with a uniform size and shape, have low environmental background level, and are chemically inert and stable in size or shape under various environmental and biological conditions.[58] Spinach was selected as the model plant because of its large consumption worldwide and large shoot surface area, which is ideal for foliar study.

3.2 Materials and Methods

3.2.1 Materials

Gold(III) chloride trihydrate and hydroquinone were purchased from Sigma-Aldrich (St. Louis, MO). Sodium citrate dehydrate was purchased from Fisher Scientific (Pittsburgh, PA). Organic spinach leaves were purchased from a local grocery store in Amherst, MA and transferred to the Chenoweth Lab at University of Massachusetts Amherst. All spinach leaves were stored at 4 °C and used within 1 day. All leaves were washed with deionized water (Barnstead MicroPure system, Fisher Scientific Co., Pennsylvania) with a pH of 6.

3.2.2 Fabrication and Characterization of Au NPs

15 nm Au NPs were synthesized by the Turkevich method and 35 to 125 nm Au NPs were synthesized by the hydroquinone reduction and seed-mediated growth method.[68]

Transmission electron microscopy (TEM, JEOL JEM-2000FX) was used to characterize the synthesized Au NPs. In order to completely disperse the Au NPs, we used probe sonicated (Branson 2800) for our Au NPs with 15 minutes before dropping on the copper grids. The sizes of synthesized Au NPs (n=100) were measured using the ImageJ Software (NIH, Bethesda, MD) based on acquired TEM images. We also measured the particle size distributions of the Au NPs samples using a dynamic light scattering instrument (Mastersizer 2000, Malvern Instruments). The surface charge of Au NPs was determined by using a particle electrophoresis instrument (Zetasizer Nano ZS series, Malvern Instruments) (Table S1). UV-vis absorption spectra of the Au NPs samples were recorded on a SpectraMax spectrophotometer (Molecular Devices, LLC., CA) in the range

350-750 nm with 10 nm resolution. Plastic cuvettes with a 1-cm optical length were used (Table S1).

3.2.3 Preparation for *in situ* Study of Au NPs Adsorbed on Spinach Leaf Surfaces

To study the Au NPs adsorbed on spinach leaf surfaces, 3 mL Au NPs of different concentrations (50 and 5 mg L^{-1}) and sizes (15, 35, 80, and 125 nm) were prepared in petri-dishes. The concentrations of the Au NPs (50 and 5 mg L^{-1}) used in this study are based on the concentrations of Ag NPs currently used in the commercial pesticide products in the US market. Then, fresh spinach leaves were immersed into these solutions and incubated for 30 minutes on the Fisher Scientific^{TM} Nutating Mixers (Fisher Scientific Co., PA) at the low speed of 24 rpm to ensure the leaves fully exposure to Au NPs. After that, the leaves were gently rinsed with deionized water for 3 minutes and air-dried in the hood under room temperature. Spinach leaves without Au NPs were used as a control. Bright field light scattering images, Raman images, and representative Raman spectra were then collected.

3.2.4 Preparation for *in situ* study of Au NPs Penetrated into Spinach Leaves

To study the penetration of Au NPs into spinach leaves, 10 μL Au NPs (50, 200 mg L^{-1}) were dropwise deposited on the leaf surfaces in predetermined areas. The spinach leaves that were treated with Au NPs were air-dried in the hood at room temperature. Raman images, and representative Raman spectra were collected immediately.

3.2.5 Raman Instrumentation and Data Aanalysis

A DXR Raman microscope (Thermo Fisher Scientific, Madison, WI) with a 780 nm laser and 10×, 20× confocal microscope objectives were used in this study. Each spectrum was scanned from 3400 to 400 cm^{-1} with 5 mW laser power and 2s exposure

time. Raman maps were integrated based on the characteristic peaks in the Raman spectra using the atlμs function in the OMINCS software (Thermo Fisher Scientific). For the surface study, Raman mapping was applied with a 50 μm slit aperture to maximize the signals. To compare Raman and optical images, the step size is 10 μm step size and each image contains 100 spots. To map Au NPs of different sizes (15-125 nm), the step size is 40 μm and each image contains 360 spots. In this way, we can quickly scan the representative area within 30 min. For the penetration study, Raman mapping was applied with a 50 μm pinhole aperture to control the confocal depths. The step size in X direction is 10 μm and in Z direction is 10 μm, and each image contains 150 spots. The instrumentation parameters (laser power and exposure time) were optimized to achieve sensitive and rapid detection without damaging the leaf tissues.

3.2.6 Transmission Electron Microscopy Characterization of Au NPs in Spinach

Au NPs distribution in spinach leaves was observed by TEM (JEOL, JEM-2200FX). Spinach leaves were prepared by fixation, dehydration, infiltration and polymerized at 60 °C for 24 hours.[69] The ultrathin sections (90 nm) were cut and placed on the grid. Finally, TEM (200 kV) was used to observe the specimens.

3.3 Results and Discussion

3.3.1 In situ Detection and Characterization of Au NPs on Spinach Leaves

Figure 3.1a and 3.1c show bright field light scattering images of spinach leaves without and with Au NPs (35 nm, 50 mg L^{-1}). As shown in Figure 3.1c, Au NPs were heterogeneously distributed on the spinach leaves' surfaces. This uneven distribution of Au NPs is likely due to the complex structures of the spinach leaves' surface. The bright color of Au NPs is a result of their surface plasmon (SPR).[70] Figures 3.1b and 3.1d are the

corresponding Raman images which were constructed based on the highest peak at ~1525 cm^{-1}. The peak assignments for the normal Raman spectra of carotenoids and plant leaves have been previously reported.[71,72] Three major peaks (1525, 1156 and 1005 cm^{-1}) have been identified as carotenoids, which are presented in the plant leaves. Among these three peaks, the 1525 cm^{-1} is the largest. We also extracted all the pigments (chlorophylls and carotenoids) and measured their SERS signals. Our results (Figure 3.2) agreed with the references. Therefore, the 1525 cm^{-1} peak is most likely from carotenoids. As in other imaging techniques, it is critically important to identify and subtract background signals to minimize matrix interference. Here we set 200 counts (at 1525 cm^{-1}) as the baseline for background subtraction for the best results with 2% false positive and 5% false negative (Figure 3.3). As shown in Figure 3.1d, when Au NPs were on the leaves, spots with higher intensity were clearly shown in different colors other than blue, which indicates the presences of Au NPs on leaf surfaces. These Au NPs are mainly Au NPs aggregates, as individual Au NPs have very weak enhancement.[73] The spectra varied from spot to spot with different patterns and intensities, indicating that the Au NPs distribution and local environment of Au NPs were quite heterogeneous. In addition, the non-flat surface would also result in the orientation difference between the laser and Au NPs, which would contribute to the spectral variance. The assignment of SERS peaks is very difficult compared with normal Raman, as molecules can interact with NPs in many different ways. Generally speaking, only the molecules adsorbed (interacted) on the Au NPs were most enhanced. This is because the enhancement is highly distance dependent. Other molecules may be surrounding the Au NPs; however, if the distance is larger than ~10 nm, there is no enhancement at all.[74] The selected SERS spectra (Figures 3.1f and 3.1g) show enhanced

peaks that are similar to the normal Raman spectra (Figure 3.1e), which indicates the interactions between the Au NPs and leaf chlorophylls and carotenoids. To verify this, we extracted chlorophylls and carotenoids from spinach leaves and mixed them with Au NPs. The resulting SERS spectra (Figure 3.2) show similar characteristic peaks to the *in situ* spectra (Figures 3.1f and 3.1g), demonstrating the interaction between Au NPs and plant pigments *in situ*. In the literature review, we found two possible mechanisms for the interaction between Au NPs and chlorophylls. One study indicates the negatively charged Au NPs are bound to the magnesium metal center of chlorophylls, which is coordinatively unsaturated.[75] Another study demonstrates the formation of Au NPs and chlorophylls complex is due to the ligand-exchange reaction between Au NPs and nitrogens of chlorophylls via nonbonding electrons.[76] The binding constant for Au NPs and chlorophyll is very high, ~ 10^5 M^{-1} and the amount of chlorophylls in spinach leaves is about 1-2%.[77] Therefore, chlorophylls are highly likely to interact with Au NPs and thus be reflected in the SERS spectra. Other peaks have been observed too, which indicates the complexity of the biomolecules co-adsorbed or close to the Au NPs. For example, some carotenoids peaks were observed in the *in situ* spectra as well. In addition, a peak at 2130 cm^{-1} was observed after the application of Au NPs on spinach leaves. Since no peak at 2130 cm^{-1} was observed on spinach leaves without Au NPs, we assume this peak may come from Au NPs, which may prove that the spectra we obtained are involved with Au NPs. The origin of this peak is unknown. In addition, some spots with high intensity (e.g. Figure 3.1h) were also observed. The SERS spectrum of hot spot was significantly different than the others, with broader shifts at around 1000-1700 cm^{-1}. This may be due to significant aggregation of NPs that produced stronger and multiple localized SPR which enhanced and broadened the

carbon peaks and thus reduced the characteristic information. We observed a similar phenomenon when measuring Au NPs aggregates on a gold coated glass slide (Figure 3.4). Although those super-hot spots can be used to determine both the presence and aggregation state of Au NPs, the characteristic information of the NPs-leaf interactions may not be reflected.

Given the limitation of all the micro-imaging techniques, we could only look at a small area under the Raman microscope. Therefore, it is important to select an area that is statistically representative of the entire target. Though we can scan at a very fine step over the entire leaves to collect all the information, it is too time-consuming, impractical, and not statistically meaningful. Comparing the Raman image with the optical image, we found most parts of these two images matched fairly well. Most of the Au NPs shown in the optical image also produced signals in similar positions in the Raman image, though some spots were missed because the set step size (10 μm) is larger than the laser spot (3 μm). The intensity of the Au NPs in these two images did not correlate. The intensity of Au NPs in the optical image is mainly based on the amount, while the intensity of SERS signals also depends on some different factors, such as amount, aggregation, and interactions. In addition, since the surfaces of spinach leaves are not flat, in a scanning area, some parts of the area may be in focus and some may be out of focus. Thus, if the part of the scanning areas is out of focus, even with a large amount of Au NPs, the SERS signals may also be weak. In addition, some undetected NPs not shown in the optical image were detected by using SERS, probably due to the penetration ability and increased sensitivity of the laser. Compared with our previous study that used a Raman reporter (ferbam) as the indicator to detect and quantify Ag NPs in liquid and semi-liquid matrix,[9] no indicator was used in this

study. This is because the purpose of this study is not only to detect the Au NPs, but also to investigate whether we are able to characterize the interactions between the Au NPs and plant biomolecules based on the SERS signals. If an indicator was used, the sensitivity and quantitative ability of detection may be improved; however, we lose the information about plant-NPs interactions.

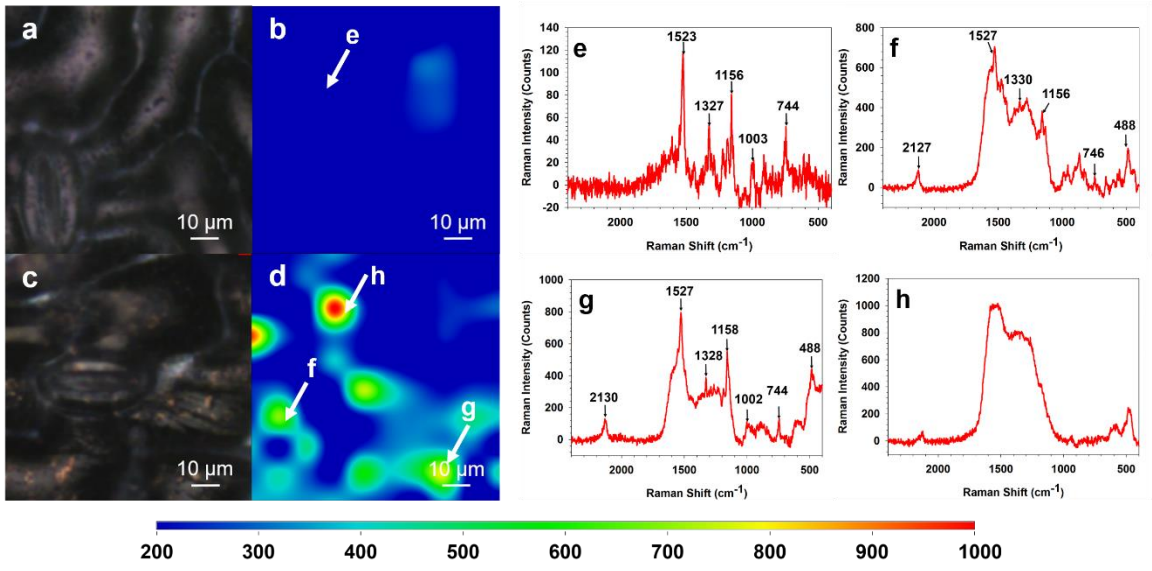

Figure 3. 1 Bright light scattering images, Raman images, and Raman spectra of spinach leaf with and without 35 nm Au NPs. (a) and (b), bright light scattering image and Raman image of spinach leaf without Au NPs. (c) and (d), bright light scattering image and Raman image of spinach leaf with Au NPs. (e)-(h), Raman spectra of selected spots on Raman images. The step size of the mapping is 10 μm and one image contains 100 scanning spots.

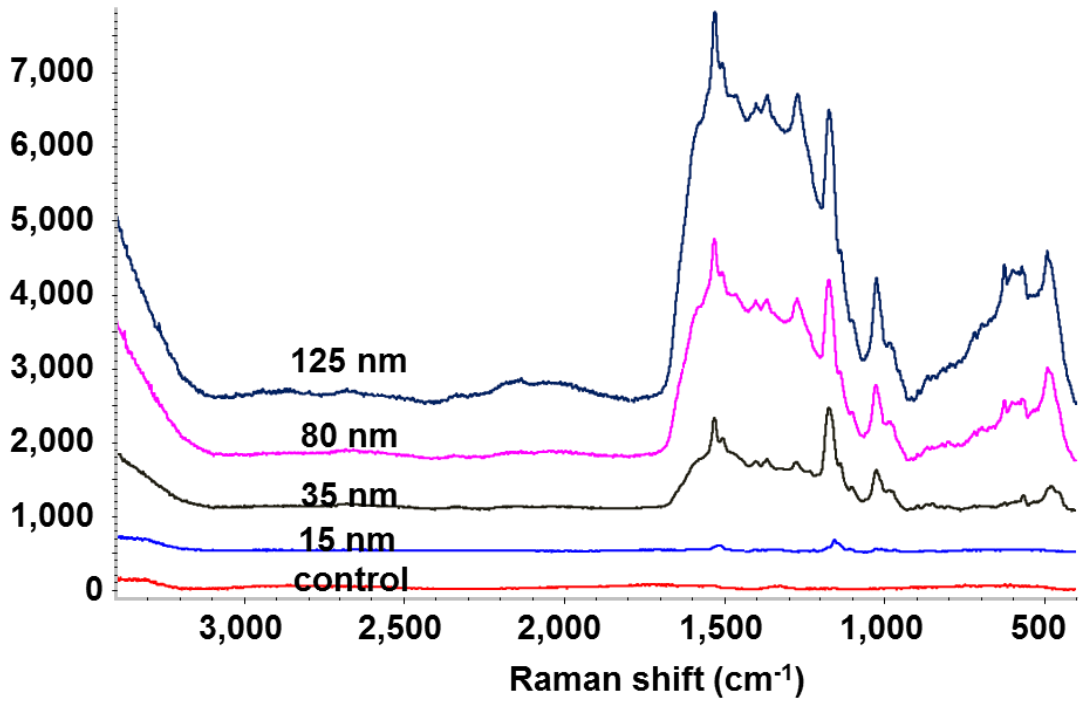

Figure 3. 2 SERS spectra of pigments (chlorophylls and carotenoids) extracted from spinach leaves mixed with Au NPs of different sizes (15-125 nm). The detailed extraction was adapted by a published protocol as follows. 100 μL extracted solu*t*ions (500 mg L^{-1}) were mixed with 100 μL Au NPs at 50 mg L^{-1} for 30 min, then the Au NPs were deposited on a gold coated glass slide for Raman measurement. Compared with control (just pigments without Au NPs), all the Au NPs show enhanced signals. The SERS spectra obtained was found similar to the *in situ* SERS spectra of Au NPs on and in spinach leaves, indicating the Au NPs were interacted with plant pigments on and in spinach leaves. 15 nm Au NPs shows the least enhancement, while the 125 nm Au NPs show the most enhancements. The similar size dependent SERS enhancement was also reported in other study.[2]

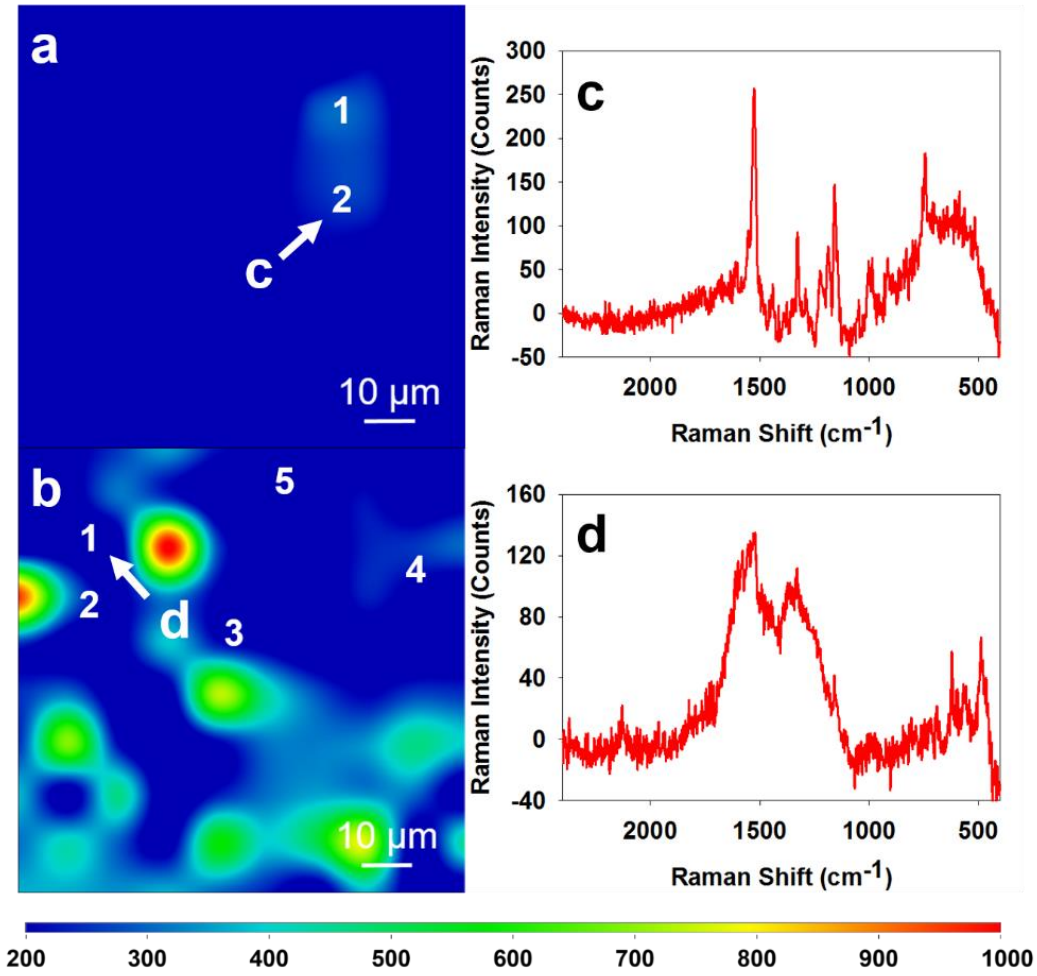

Figure 3. 3 Estimation of false positive (2%) and false negative (5%) of the mapping method with the baseline set at 200 counts based on the 1525 cm^{-1} peak. (a) 2D Raman mapping of spinach leaf without Au NPs. Two out of 100 points had higher than 200 counts, (b) 2D Raman mapping of the spinach leaf with Au NPs. Five out of 100 points contain characteristic peaks of Au NPs but had lower than 200 counts, (c) representative spectrum of the false positive signal, (d), representative spectrum of the false negative signal.

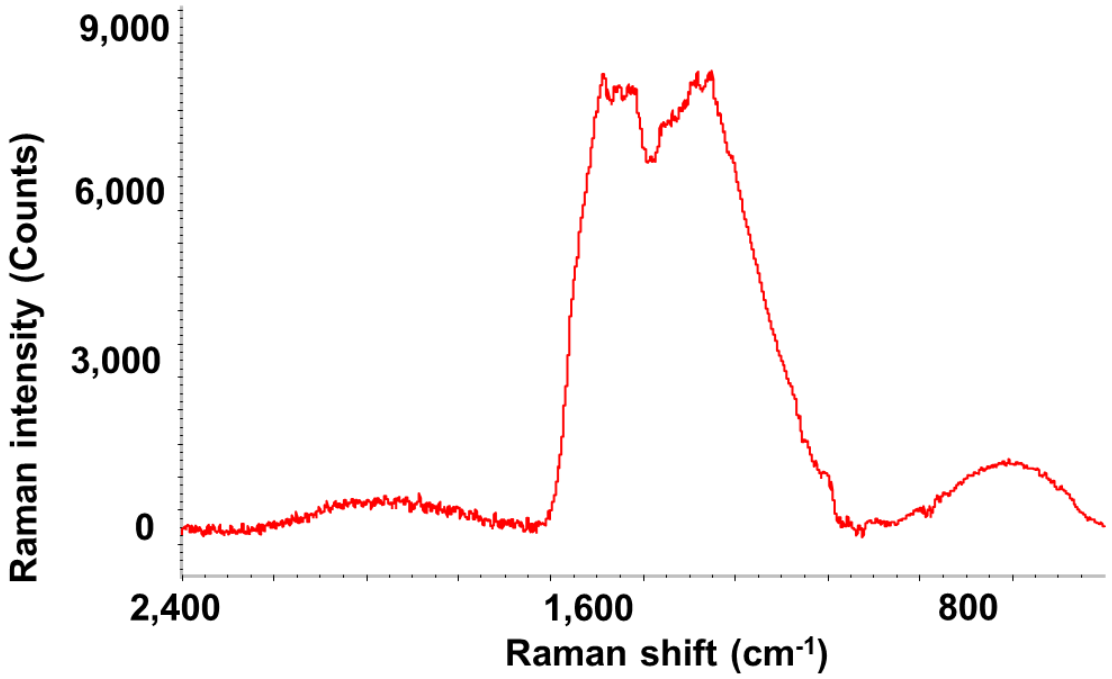

Figure 3. 4 SERS spectrum of Au NPs aggregates dried on a gold coated slide. A broad peak over 1000-1700 cm^{-1} was observed, which is similar to the *in situ* spectra observed from Au NPs on and in spinach leaves. The intensity of the signals on a gold slide was higher than that on and in spinach leaves because of the better reflectivity of the gold slide.

3.3.2 Raman mapping of Au NPs of Various Sizes on Spinach Leaves

To evaluate the mapping method for measuring Au NPs of different sizes (15-125 nm) on spinach leaves, we randomly picked an area on the leaves with the size of 920 µm × 560 µm and used a relative large step size (40 µm), which resulted in 360 spots per image. In this way, we were able to quickly scan the representative area within 30 min.

In Figures 3.5 b1-e1, after being contaminated with Au NPs at 50 mg L^{-1}, it is interesting to find that, except 15 nm Au NPs treated group, strong SERS signals were obtained from each of the other three groups, which indicates the presence of Au NPs on

these spinach leaves. The intensity of SERS signals is strongly determined by the following aspects: 1) the aggregation status (hot spots) of Au NPs; 2) the size of Au NPs in the aggregation; and 3) the number of NPs in the probed area. In this study, we deposited different sizes of Au NPs under the same mass, which means the number of Au NPs with smaller size is larger than those with bigger size. As shown in Table S1, 15 nm NPs have the lowest SPR, therefore, they have the least enhancement factor even in the aggregation status. Although their number is the largest, it is still very challenging to detect them. Furthermore, when we decreased the concentration of Au NPs to 5 mg L^{-1} (Figure 3.5 b2-e2), although SERS intensity became weaker, 35, 80 and 125 nm Au NPs were still detectable *in situ*. This data demonstrated that we were able to map various sizes of Au NPs on spinach leaves *in situ*. Although increasing exposure time and/or laser power may enhance the sensitivity, it may cause potential damage to the leaves and significantly increase the time for image analysis using this mapping technique.

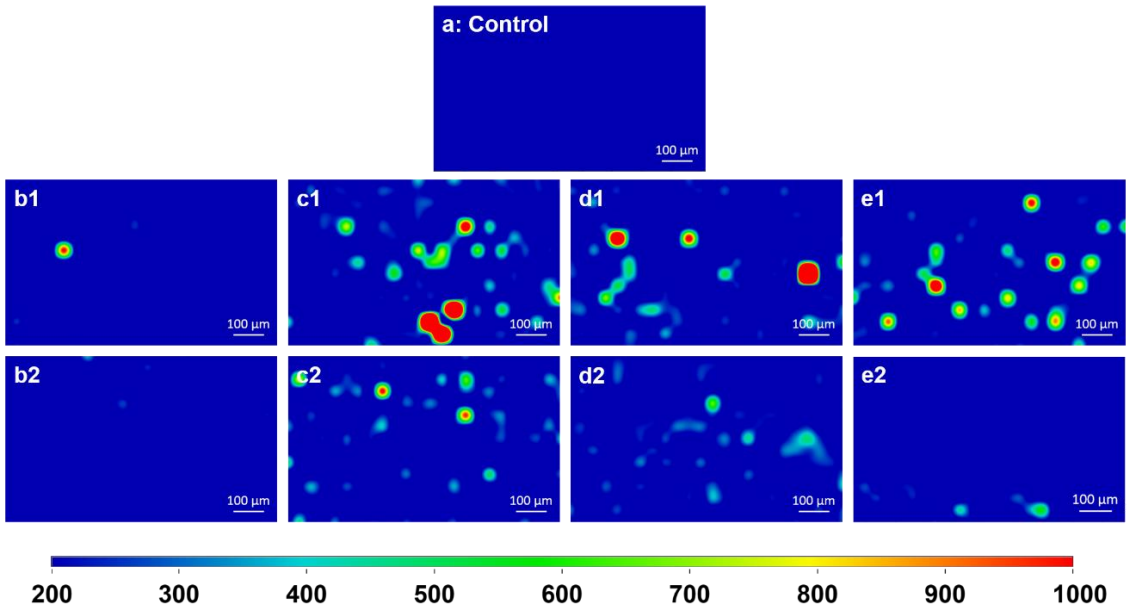

Figure 3. 5 Raman images of spinach leaves with Au NPs of different sizes (15-125 nm) and concentrations (50 and 5 mg L^{-1}). (a), spinach leaves without Au NPs. (b1)-(e1), spinach leaves with 50 mg L^{-1} Au NPs of different sizes. (b2)-(e2), spinach leaves with 5 mg L^{-1} Au NPs of different sizes. Step size is 40 μm and one image contains 360 scanning points.

3.3.3 *In situ* Detection and Characterization of Au NPs in Spinach Leaves

There are two non-destructive approaches of using the confocal Raman spectroscopy to detect and characterize Au NPs in spinach leaves *in situ*. The first approach is to scan the area maps (XY) at different depth. Figures 3.6 a-c show the Raman images of three different depths (0, 10, and 20 μm). Hot spots with strong signals in 10 μm and 20 μm depth image were clearly observed, indicating that Au NPs were able to penetrate into the spinach leaves. Compared with 0 and 10 μm images, the number of spots with high intensity significantly decreased at 20 μm depth, which means there are decreasing amounts and less aggregation of Au NPs in deeper areas. Looking into the selected SERS spectra at different depths, the 0 and 10 μm spectra (Figures 3.6 d and 3.6 e) do not have characteristic peaks but a broad peak between 800-1600 cm^{-1}, which indicates the NP-NP interaction (aggregation), while the spectrum of Figure 3.6 f shows clear enhanced peaks of carotenoids and chlorophylls, which demonstrates NP-pigment interactions. We also characterized other spots in the 20 μm depth images and found most of them showing various patterns combining the characteristic peaks of carotenoids and chlorophylls (Figure 3.7). This indicates strong interactions between Au NPs and plant pigments.

The second approach is to scan the area map vertically (XZ) to get more direct information on the penetration depth of Au NPs. Based on the previous report, it was

estimated that the thickness of a spinach leaf was normally from 300 to 600 μm.[7]> Thus, we scanned from the top to 300 μm in depth to study the penetration depth of 35 nm Au NPs. Multiple images were collected randomly on the leaf surfaces, and three representative images were shown in Figures 3.6 h-j. Compared to the control (without Au NPs), these images show enhanced signals though varied with penetration depth from 80-150 μm. The variation of the penetration depth may be caused by spatially heterogeneous leaf structures and properties, including spinach leaves' wax coverage, surface wettability, stomata geometry and permeability, and so on.[80,81] Several studies demonstrated that stomatal[81] and cuticular pathways[51,52] may enable ENPs accumulation in plant leaves through foliar exposure. In this study, we observed both pathways for Au NPs penetrating into spinach leaves as shown in Figure 3.9. In terms of penetration depth, there is no significant difference between these two pathways. But stomata may allow more Au NPs to penetrate in some cases, as indicated by intense signals observed in the depth image.

We also did a validation study by cutting the leaf and scanning the cross-sections. As shown in Figure 3.10, the strongest SERS intensity was observed mainly at around 30 μm depth. With the depth increasing, although the Raman intensity in each layer became weaker, up to 240 μm, the intensity of Raman spectrum was still around 400 counts. The depth profile obtained from this method is deeper than the previous method. One possibility is the under-estimation of the confocal scanning, which resulted from decreased penetration ability of laser at further depth and heterogeneous structure of spinach leaves.[8]> However, the result from the cutting method may be over-estimated as the pressure of cutting may artificially enhance the Au NPs' accumulation. Nevertheless, it may not be practically meaningful to estimate the absolute penetration depth. These results

demonstrate that the Raman mapping technique can be used to measure Au NPs in spinach leaves *in situ*.

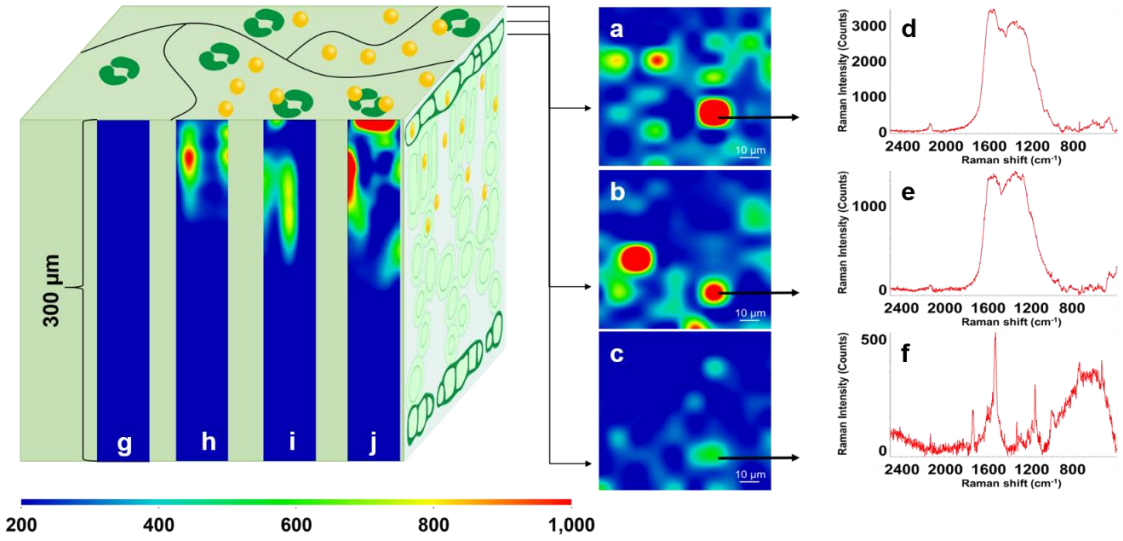

Figure 3. 6 Raman images and selected SERS spectra of Au NPs in spinach leaves. (a)-(c), Raman images in different depth profile (0, 10, and 20 µm). (d)-(f) are SERS spectra at the same spot in different depth profile (0, 10, and 20 µm). (g), Raman depth image of spinach without Au NPs. (h)-(j) are Raman depth images of spinach with Au NPs. For surface mapping (a-c), the step size is 10 µm and each image contains 100 spots. For depth mapping (h-k), the step size in X direction is 10 µm and in Z direction is 10 µm, and each image contains 150 spots.

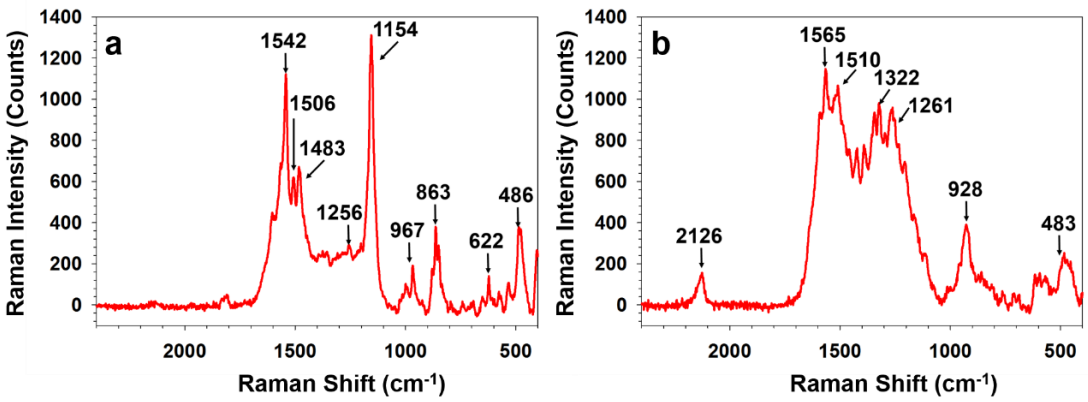

Figure 3. 7 SERS spectra of different spots in spinach leaves at 20 µm depth *in situ*. They show different patterns combining the characteristic peaks of carotenoids and chlorophylls, as well as the sulfur peaks, which demonstrate the strong interactions with plant pigments and sulfur containing compounds.

3.3.4 Raman Mapping of Au NPs of Various Sizes in Spinach Leaves

We then applied the vertical mapping approach to study the size effect on NP penetration. Four sizes (15, 35, 80, and 125 nm) and two concentrations (50 and 200 mg L^{-1}) were used. For each size and concentration, at least five mappings were collected below the cuticle. The deepest penetration depth images were shown in Figure 3.8. Au NPs of all sizes can penetrate into spinach leaves to different depths. In addition, we observed a size dependent penetration effect. The 125 nm Au NPs were found remaining mostly close to the surface, while the 80 and 35 nm Au NPs penetrated into approximately 100 and 150 µm in depth, respectively. This is probably due to the diffusion coefficients, which are inversely proportional to the radius of the permeant.[3,8]> Thus, it is reasonable to hypothesize that the part of Au NPs that penetrated into deep area might come from the Au NPs with smaller size. The reason for the low penetration depth of 15 nm observed in the

image is likely due to the weaker signals from 15 nm which made it difficult to track these Au NPs in deeper depth, although they may penetrate the deepest. In addition to the size effect, we observed the Au NPs at higher concentrations penetrated deeper than lower concentrations and the signal intensities were higher than those of low concentrations in the Raman images. One study also found a similar effect of concentration on the penetration depth.[83] However, this may also be influenced by the sensitivity of the SERS mapping techniques which captured more signals when the concentration was higher.

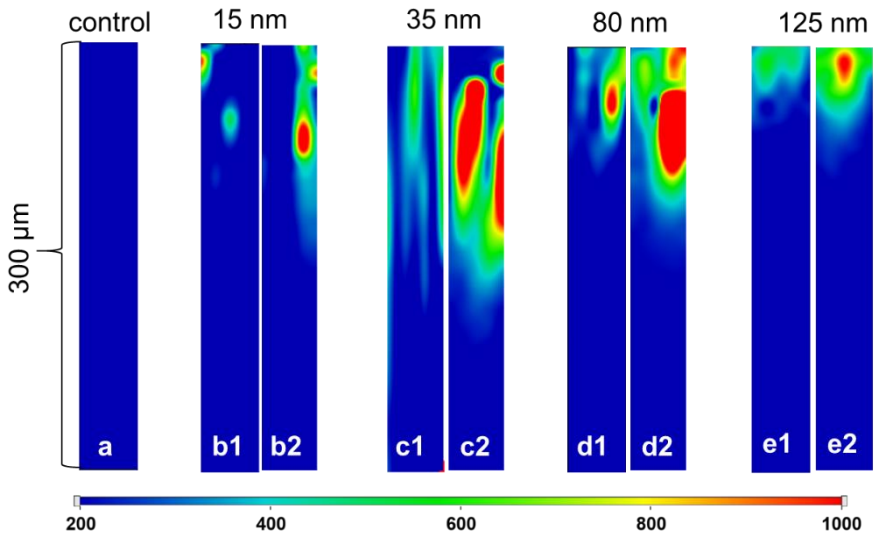

Figure 3. 8 Raman images of Au NPs with different sizes (15-125 nm) and concentrations (50 and 200 mg L^{-1}) in spinach leaves. (a), spinach leaves without Au NPs. (b1)-(e1), spinach leaves with 50 mg L^{-1} Au NPs of different sizes. (b2)-(e2), spinach leaves with 200 mg L^{-1} Au NPs of different sizes. The step size in X direction is 10 µm and in Z direction is 10 µm, and each image contains 150 spots.

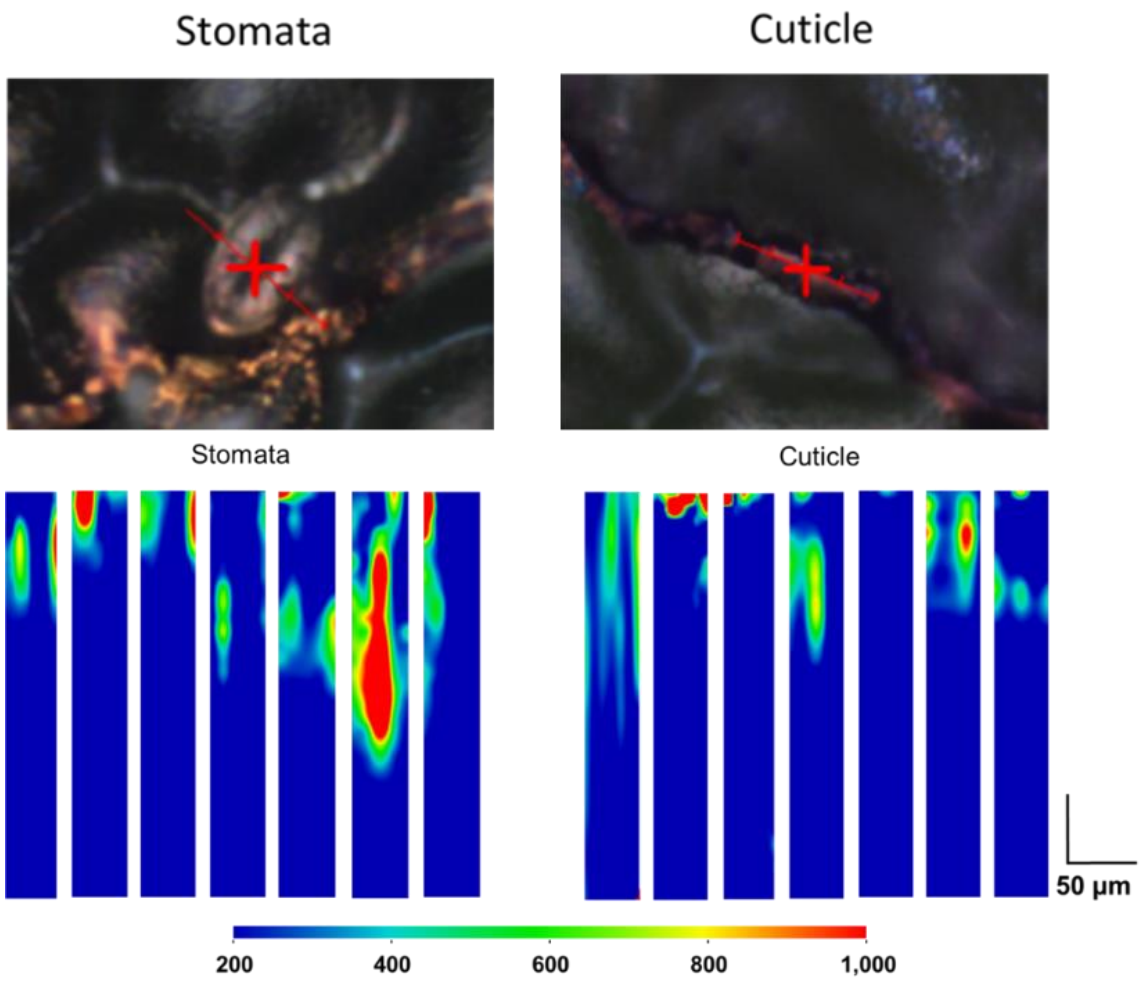

Figure 3. 9 Optical images of representative selected areas for studying stomata and cuticle penetration, and SERS mapping of penetration depth profiles of 35 nm Au NPs through randomly picked stomata and cuticle on spinach leaf surfaces. Both of these two penetration pathways show variations in term of penetration depth, and there is no statistical difference between them. Stomata may allow more Au NPs to penetrate in some cases, as indicated by intense signals observed in the depth profile.

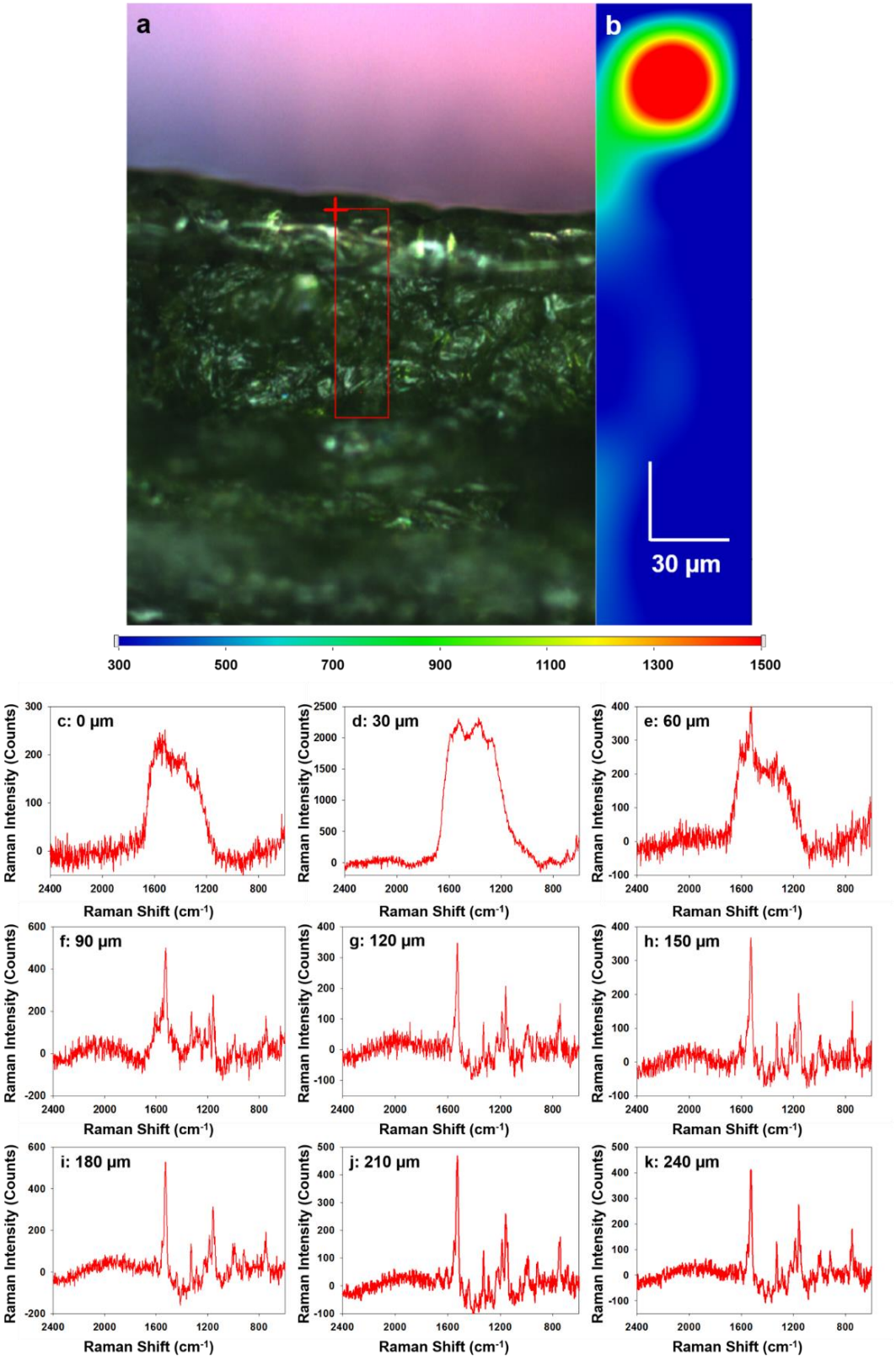
a
b
30 μm
300
500
700
900
1100
1300
1500
c: 0 μm
d: 30 μm
e: 60 μm
f: 90 μm
g: 120 μm
h: 150 μm
i: 180 μm
j: 210 μm
k: 240 μm
Raman Intensity (Counts)
Raman Shift (cm-1)

Figure 3. 10 Optical (a) and 2D Raman mapping (b) of the cross section of the spinach leaves deposited with 35 nm Au NPs. (c-k) SERS spectra collected from different depths.

3.3.5 Validation of the SERS Mapping Using TEM-EDS

To validate the SERS mapping results, TEM-EDS was used to observe and confirm Au NPs in spinach leaves. Figures 3.11 a and b show TEM images in a vertical section of a spinach leaf treated with 35 nm Au NPs (200 mg L^{-1}). It was found that Au NPs penetrated into the spinach leaf interior and were distributed both outside and inside of the leaf cell walls. Furthermore, a considerable amount of NPs was distributed in and around the chloroplasts, structures that contain mainly chlorophylls and carotenoids. This may further confirm the strong signals from plant pigments observed in the previous Raman spectra. In addition, many Au NPs were shown in aggregated status inside the leaf tissues, which also confirms the observation from previous Raman spectra. Other studies also reported that certain ENPs can attach to the surface of chloroplasts[8]> and even enter chloroplasts.[85]

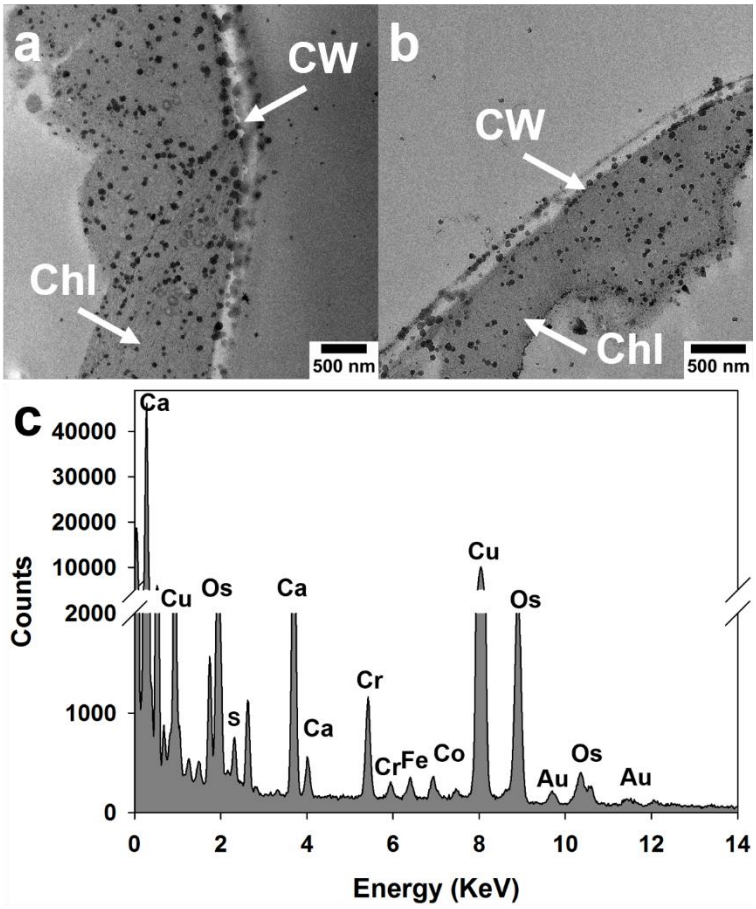

Figure 3. 11 TEM-EDS images of spinach leaves treated with 35 nm Au NPs (200 mg L^{-1}). Chloroplast (Chl) and Cell wall (CW).

3.4 Conclusion

In this current work, we developed an innovative, simple, and rapid approach using SERS mapping technique to detect and characterize different sizes of Au NPs on and in spinach leaves *in situ*. The detection was based on the hot spots produced by Au NPs on and in spinach leaves which can be clearly captured using Raman mapping without any sample preparation steps. The intensity and spectral pattern of hot spots reveal NP aggregation status as well as the interactions between Au NPs and plants. The Raman intensity of characteristic peaks from chlorophylls and carotenoids were enhanced, which

indicates the interactions between Au NPs and these plant bio-components. TEM-EDS also verified the interaction between Au NPs and chloroplast. To the best of our knowledge, it is the first study that explored and applied SERS mapping for detection and characterization of NP contaminants attaching onto and internalizing into fresh produce. We foresee this effective and transformative technique to open a new and exciting analytical window for rapidly detecting the presence of ENPs (especially Au, Ag, and Cu) in complex biological samples (such as plant leaves, biofilm, human and animal skins, etc.). More importantly, the interactions of ENPs with bio-components *in situ* can be investigated, which will greatly facilitate the understanding of ENPs' adhesive and uptake mechanisms, and further promote the understanding the behavior and fate of ENPs. We will further explore and apply this method to future studies of other ENPs (e.g., Ag and Cu NPs) and their interactions with plant tissues.

CHAPTER 4

EVALUATION OF POSTHARVEST WASHING ON AGNPS REMOVAL FROM SPINACH LEAVES

4.1 Introduction

Silver nanoparticles (AgNPs) has been known for its unique antimicrobial and insecticidal properties over 100 years.[1] For example, numerous studies on the toxicity of AgNPs to different bacterial species, including *E. coli*, *Bacillus subtilis*, *Nitrosomonas europaea*, *Pseudomonas fluorescens*, and *Pseudomonas aeruginosa*, have been performed in detail.[2] Based on these facts, AgNPs has been adopted commercially across a wide spectrum of agriculture, food, and biomedical applications.[1,>] It is estimated that the global production of AgNPs can reach 500 tons per year and significant increases are anticipated in the future.[86] Up to date, it has been reported that around 110 AgNPs-containing products had been registered as pesticides by the EPA for the purpose of medical, agricultural, environmental, and home purpose.[4] In addition, several patent applications for AgNPs-based fungicides had also been filed in the US.[4,5] However, the widely use of AgNPs-based pesticides may increase the likelihood of human exposure, for example, unintentional consumption of AgNPs contaminated crop plants, which may pose risks to human beings. So far, the toxicity of AgNPs to human cells, such as oxidative stress, genotoxicity, and apoptosis have been demonstrated by several studies. For example, after 24 h treatment, 5-10 nm AgNPs with concentration from 0.05 mg L^{-1} to 20 mg L^{-1} could result in oxidative stress, DNA damage, cell cycle arrest and apoptosis in human jurkat cells.[7] Therefore, understanding the biotransformation and distribution of AgNPs in plants is a prerequisite.

Up to now, the biotransformation and distribution of metal-based NPs inside plants after foliar exposure has been reported in several studies. Shi et al. used transmission electronic microscopy (TEM)-energy dispersive spectrometry (EDS) to determine the presence of CuO NPs in the intercellular space or protoplast of *Elsholtzia splendens* after foliar and root exposure.[8]> In addition, with the aid of X-ray absorption spectroscopy (XAS), they also found the conversion of CuO NPs to Cu-alginate, Cu-oxalate, and Cu-cysteine in *Elsholtzia splendens*.[87] Similarly, Larue et al. showed that TiO_2 NPs was internalized in lettuce leaves and could be observed in all types of tissues after foliar exposure.[52] Besides, through Micro X-ray fluorescenc (μXRF) and XAS, they also demonstrated the *in planta* accumulation of TiO_2 in cucumber was crystal phase dependent. For example, anatase-TiO_2 NPs was found predominantly in the xylem and cortex, while rutile-TiO_2 NPs was accumulated in phloem of exposed cucumber.[52] With regard to the exposure of plant leaves to AgNPs, limited studies have been performed. Larue et al. demonstrated that AgNPs can be entrapped by the cuticle, further penetrate through stomata and finally be distributed in various regions of the leaves. Furthermore, they showed that these internalized AgNPs would be oxidized as well as be complexed by thiol-containing molecules. However, in Larue et al. experiment, they only studied uncoated AgNPs, which is not commonly be used in real applications due to the fact that uncoated AgNPs is easily to form aggregation. More importantly, considering the limitations of instruments (μXRF and μXANES) they used, such as complex sample preparation, it is impossible to monitor the *in situ* and real time biotransformation and distribution of AgNPs in plants.

The objective of this study is to determine the *in situ* and real time biotransformation and distribution of AgNPs with different sizes (40 and 100 nm) and surface coating (citrate and polyvinylprrolidone) in spinach leaf. Due to the fact that, the most commonly used stabilizing agents in AgNPs synthesis studies were CIT (27%), followed by PVP (18%), CIT- and PVP-AgNPs were selected for this study.[8]> Spinach was chosen because of its large global consumption and high edible tissue surface area, making it an ideal model to study the foliar transfer of NP contaminants. 2D surface enhanced Raman spectroscopy (SERS) mapping technique was used to characterize the *in situ* interaction between AgNPs and plant biomolecules as well as to on line monitor the penetration of AgNPs in spinach leaf. Transmission electron microscopy (TEM) and scanning electron microscopy (SEM)-energy dispersive spectrometry (EDS) were used to validate the distribution of AgNPs in spinach leaf. This work will help us to understand the biotransformation and distribution of AgNPs in crop plants as well as to effectively evaluate the risk level associated with AgNPs contaminants in fresh produce in the future.

4.2 Materials and Methods

4.2.1 Materials

Organic spinach leaves were purchased from Whole Foods Market (Amherst, MA) and transferred to the Chenoweth Lab at University of Massachusetts Amherst. All spinach leaves were stored at 4 °C and used within 1 day. All leaves were washed with deionized water (Barnstead MicroPure system, Fisher Scientific Co., PA) with a pH of 5.85. AgNPs with different size (40 and 100 nm) and surface coating (citrate and polyvinylpyrrolidone) were purchased from Nanocomposix (San Diego, CA). Both L-cysteine (Cys) were acquired from Sigma-Aldrich (St. Louis, MO).

4.2.2 Preparation for *in situ* Study of AgNPs Penetration on Spinach

A 10 μL aliquot of the 20 mg L^{-1} AgNPs solution with different size (40 and 100 nm) and surface coating (citrate and polyvinylpyrrolidone) was dropwise added onto spinach leaf surface. All AgNPs treated spinach leaves were air-dried at room temperature. The penetration behavior of each kind of AgNPs on spinach was monitored during different time periods from 0.5 to 48 hours.

4.2.3 Determination of The SERS Characteristic Signals of Various Pesticides on Gold Coated Glass Slide

L-cysteine and glutathione (0.01 g) powder were dissolved in 10 mL deionized water (DI water) and were further diluted to 100 mg L^{-1}, respectively. DI water was used as a negative control. After that, 50 μL aliquot of each kind of AgNPs solution with 20 mg L^{-1} was added into them and mixed by a Fisher Scientific™ Analog vortex mixer (Fisher Scientific Co., PA) for 30 s, then 5 μL aliquot of mixture was transferred onto the gold coated microscope slide, and then allowed to dry at room temperature for Raman measurement.

4.2.4 Raman Instrumentation and Data Analysis

A DXR Raman microscope (Thermo Fisher Scientific, Madison, WI) with a 780 nm laser and a 20× long distance microscope objective was used in this study. Each spectrum was scanned from 400 to 3400 cm^{-1} 1 s exposure time. For determining the interaction between each kind of AgNPs and biomolecules (L-cysteine, glutathione) *in vitro*, SERS spectra were collected with a 50 μm slit aperture 5 mW laser power to maximize the signals. Eight discrete locations were randomly chosen on each sample for analysis. For penetration studies, SERS depth mapping images were acquired with a 50 μm

pinhole aperture 1 mW laser power to control the confocal depths using a scanning depth of 300 µm. Each area was randomly picked up from spinach leaf and vertical to leaf surface with 100 µm × 300 µm area. The step size of the mapping was 10 µm and one image contained 150 scanning spots. Raman images were integrated based on the characteristic peaks in the pesticide spectra using the atlµs function in the OMINCS software (Thermo Fisher Scientific, Madison, WI).

4.3 Results and Discussion

4.3.1 Interactions of Biomolecules and AgNPs in Spinach Leaf.

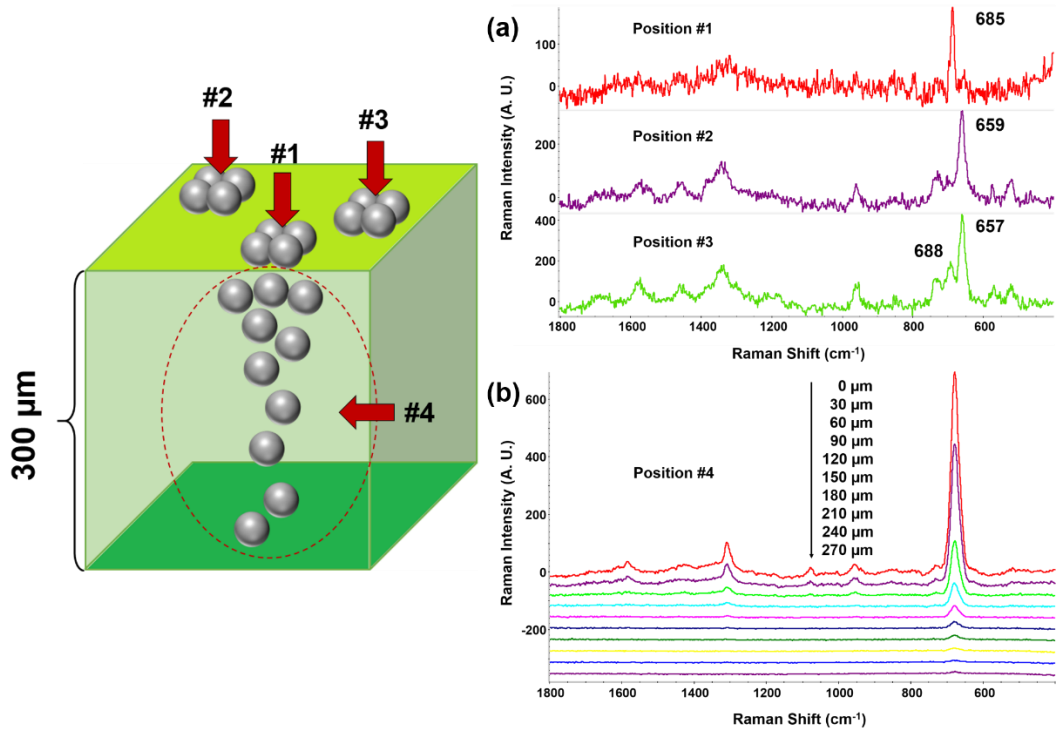

Figure 4. 1 (a) SERS spectra of 40 nm CIT-AgNPs in different position of spinach leaf; (b) SERS spectra of 40 nm CIT-AgNPs in different depth (depth: 0 to 190 µm) of spinach leaf.

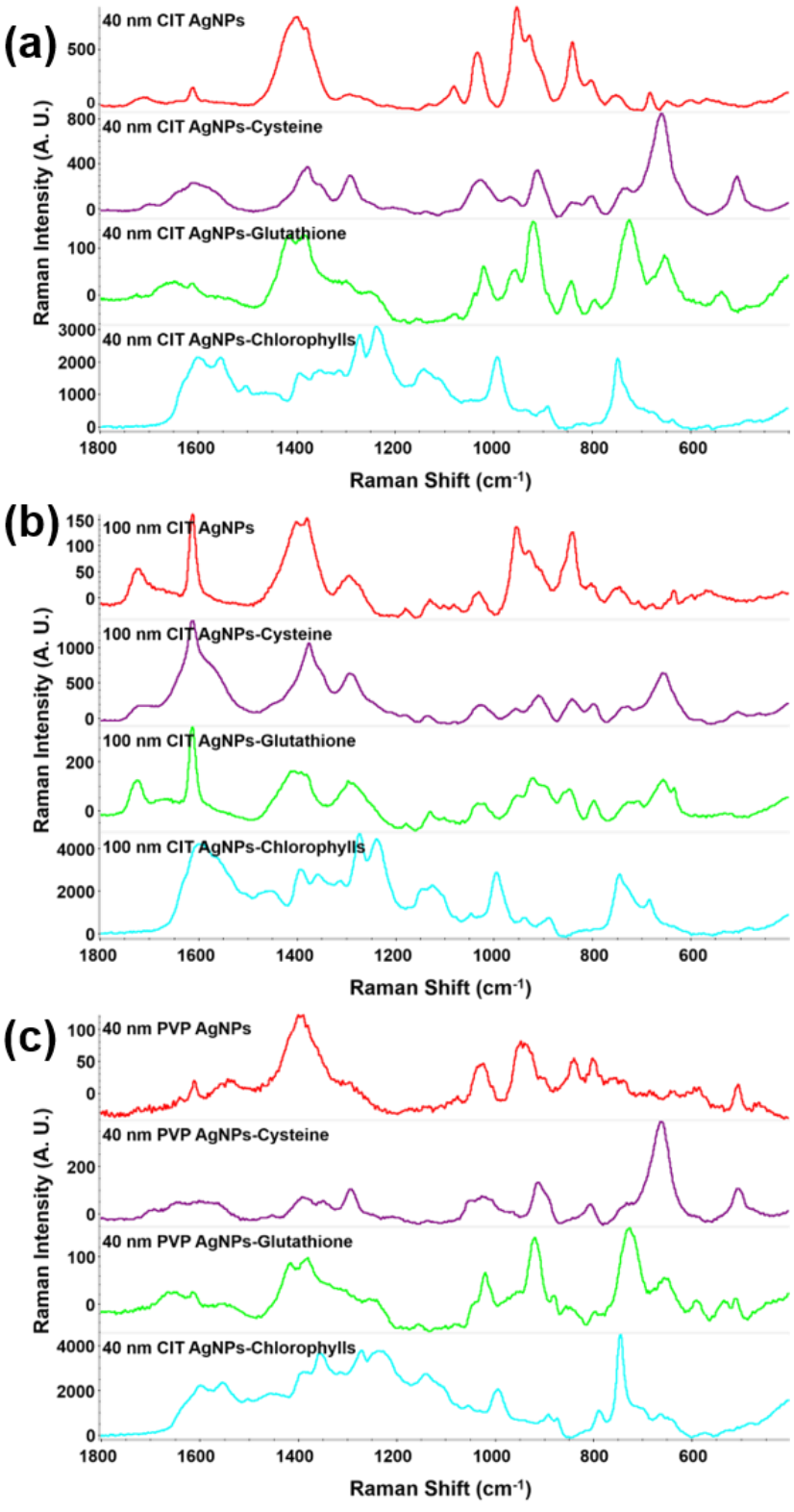
(a)
40 nm CIT AgNPs
40 nm CIT AgNPs-Cysteine
40 nm CIT AgNPs-Glutathione
40 nm CIT AgNPs-Chlorophylls
Raman Intensity (A. U.)
Raman Shift (cm-1)
(b)
100 nm CIT AgNPs
100 nm CIT AgNPs-Cysteine
100 nm CIT AgNPs-Glutathione
100 nm CIT AgNPs-Chlorophylls
Raman Intensity (A. U.)
Raman Shift (cm-1)
(c)
40 nm PVP AgNPs
40 nm PVP AgNPs-Cysteine
40 nm PVP AgNPs-Glutathione
40 nm CIT AgNPs-Chlorophylls
Raman Intensity (A. U.)
Raman Shift (cm-1)

Figure 4. 2 SERS spectra of the interactions between different biomolecules and (a) 40 nm CIT-AgNPs, (b) 100 nm CIT-AgNPs and (c) 40 nm PVP-AgNPs.

In order to investigate the interactions between AgNPs and bio-components on spinach leaf, the spectra of 40 nm CIT-AgNPs in three different positions were collected. As shown in Figure 4.1a, the spectrum collected from different location showed different pattern. The highest peaks in these three spectra are 685, 659 and 657 cm^{-1}, respectively. Although the positions of highest bands are slightly different, all these bands can be assigned to C-S stretching. The Raman shift of the highest band may originate from different localized conditions, such as desorption, re-orientation, chemical transformation of the biomolecules on AgNPs surface. It is seen that the pattern of SERS spectra collected from one position at different depth are similar. However, the SERS intensity gradually decreased with the depth increasing, which may be due to the reason that less AgNPs are present in the deeper area.

To specify what kind of biomolecule would interact with AgNPs, an *in vitro* study is needed. However, there are hundreds of thousands of bio-components in plants. In order to minimize the candidate component, understanding the possible interaction between AgNPs and bio-components in advance is necessary. when plants are exposed to extraneous AgNPs, excessive reductive oxygen species (ROS), including singlet oxygen ($^1O_2$), superoxide ($O_2^{\cdot-}$), hydrogen peroxide (H_2O_2), and hydroxyl radical ($HO^{\cdot}$) will be generated. In order to lower the toxicity of these excessive generated ROS to plants, specific defensive antioxidants that can convert these highly toxic species to less toxic species (H_2O and O_2) in plants are needed. Among a variety of antioxidants, cysteine (Cys) is a well characterized antioxidant and can prevent the stress induced by AgNPs through

thiol-group (-SH). In addition, as the primary precursor molecule in the process of glutathione biosynthesis, cysteine can be rapidly converted to glutathione (GSH) with the help of γ-glutamylcysteine (γ-ECS) and glutathione synthase (GS). These converted GSH can further scavenge ROS and be oxidized to glutathione disulfide (GSSG), which can then be recycled by glutathione reductase (GR). Furthermore, due to the presence of thiol-group, Cys, along with GSH and phytochelatins (PCs), the downstream products of GSH, can detoxify AgNPs by chelating Ag ions. In addition to these biomolecules, the interaction between AuNPs and chlorophylls has also been reported in our previous study.[8]> Thus, considering all the above facts and availability of chemical reagents, an *in vitro* study of the interaction between AgNPs and biomolecules, including Cys, GSH, and chlorophylls, were performed. The SERS spectra of AgNPs (40 and 100 nm CIT, 40 nm PVP) and these biomolecules on a gold-coated slide were showed in Figure 4.2. CIT-AgNPs exhibits Raman bands at 1085, 1024, 955, 933, 839, 798 cm^{-1}, which are consistent with previous studies.[90–92] When Cys was mixed with CIT-AgNPs and PVP-AgNPs, the enhanced Raman bands of Cys at 1608, 1293, 1033, 802, 735, 664 cm^{-1} were clearly observed. These new bands are similar to the previous studies and can be assigned to the interaction of Cys and AgNPs via the -SH group.[93–95] Among them, the highest band at 660 cm^{-1}, which comes from C-S stretching and is often used as the characteristic peak to monitor the presence of Cys.

4.3.2 Size Effect on Biotransformation and Penetration Behavior.

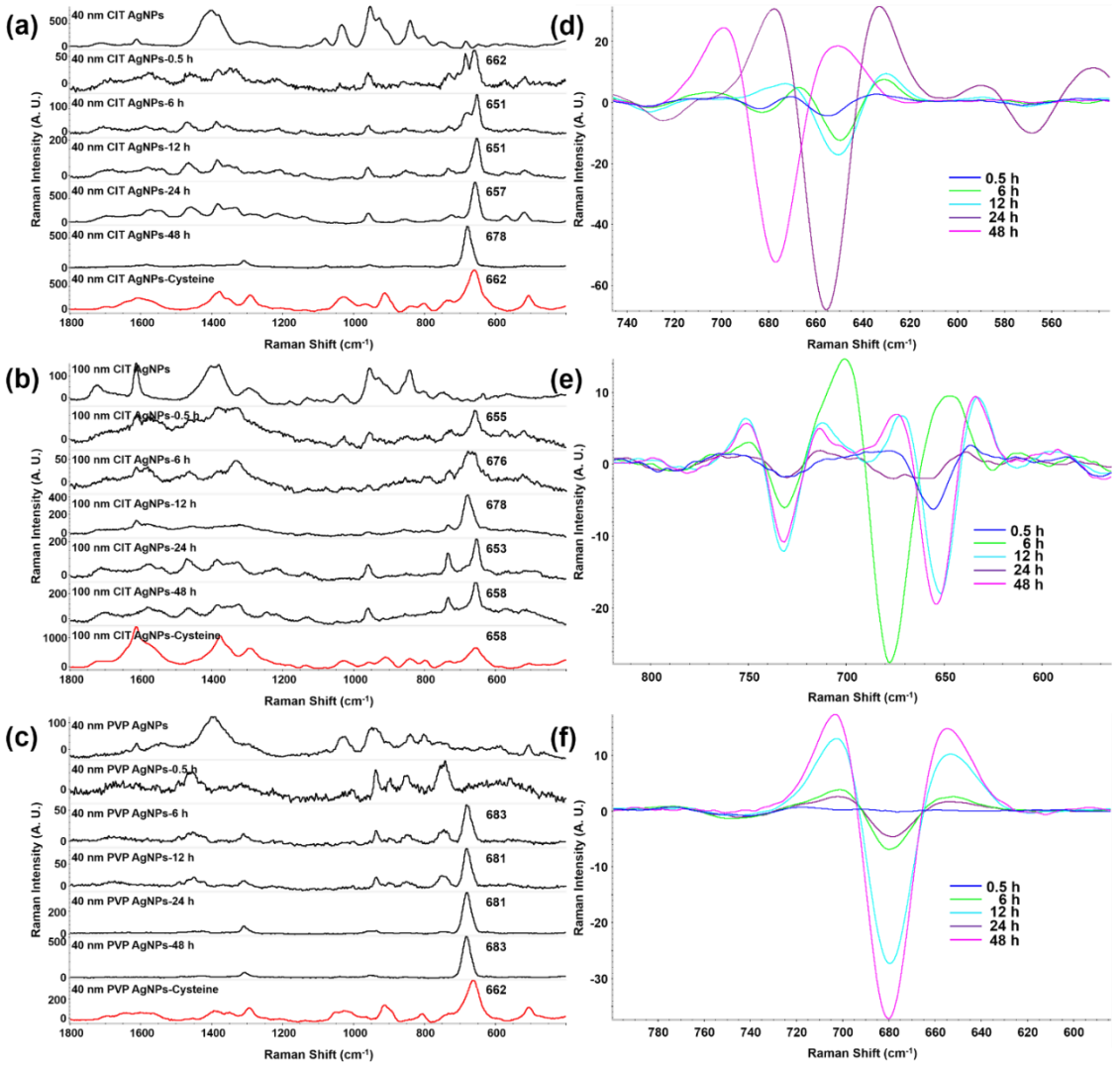

Figure 4. 3 (a), (b), (c) *In situ* SERS spectra of 40 nm CIT-AgNPs, 100 nm CIT-AgNPs, 40 nm PVP-AgNPs in spinach leaf following different exposure time; (d), (e), (f) Second derivative Raman spectra of the C-S stretching peak of cysteine from 40 nm CIT-AgNPs, 100 nm CIT-AgNPs, 40 nm PVP-AgNPs in spinach leaf following different exposure time.

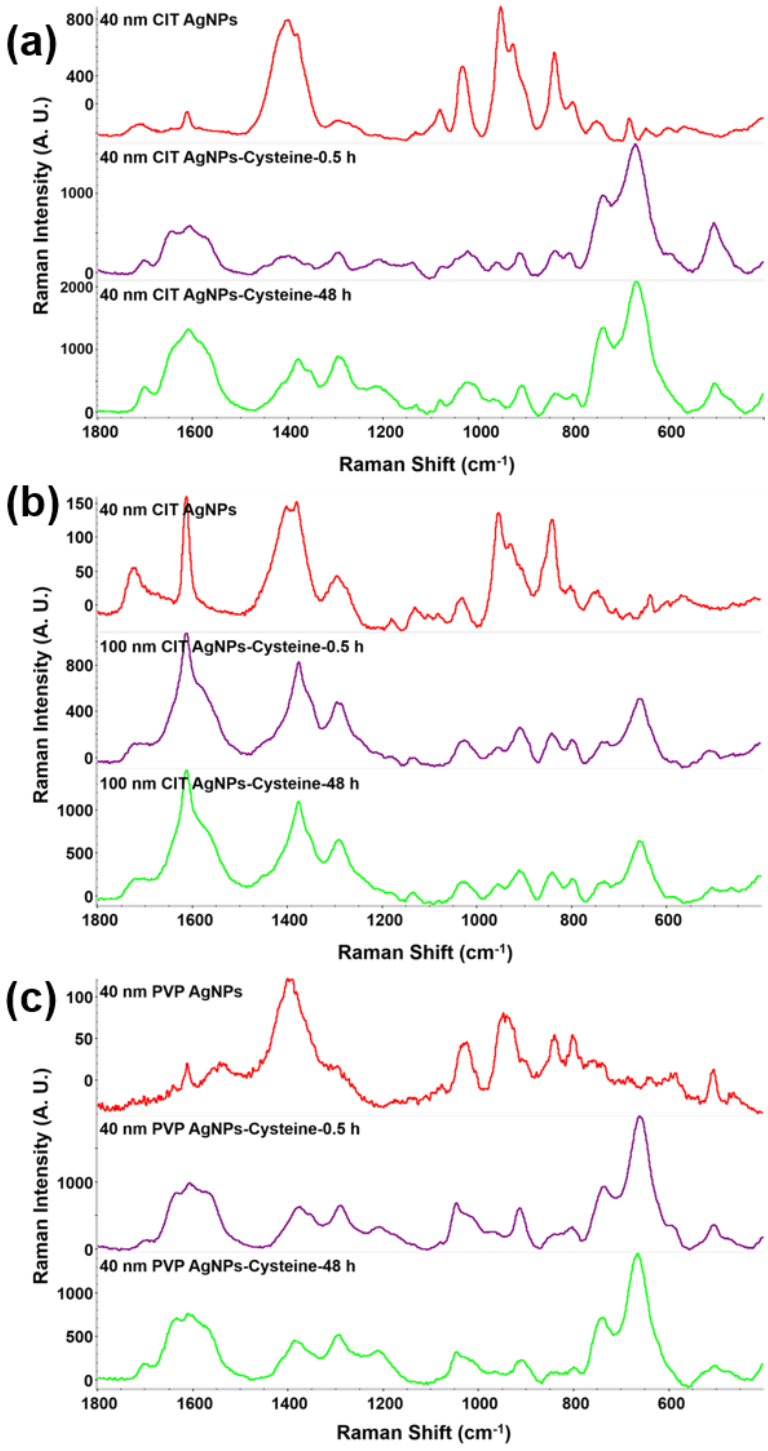

Figure 4. 4 SERS spectra of the interactions between cysteine and (a) 40 nm CIT-AgNPs, (b) 100 nm CIT-AgNPs and (c) 40 nm PVP-AgNPs following different time (0.5 and 48 h).

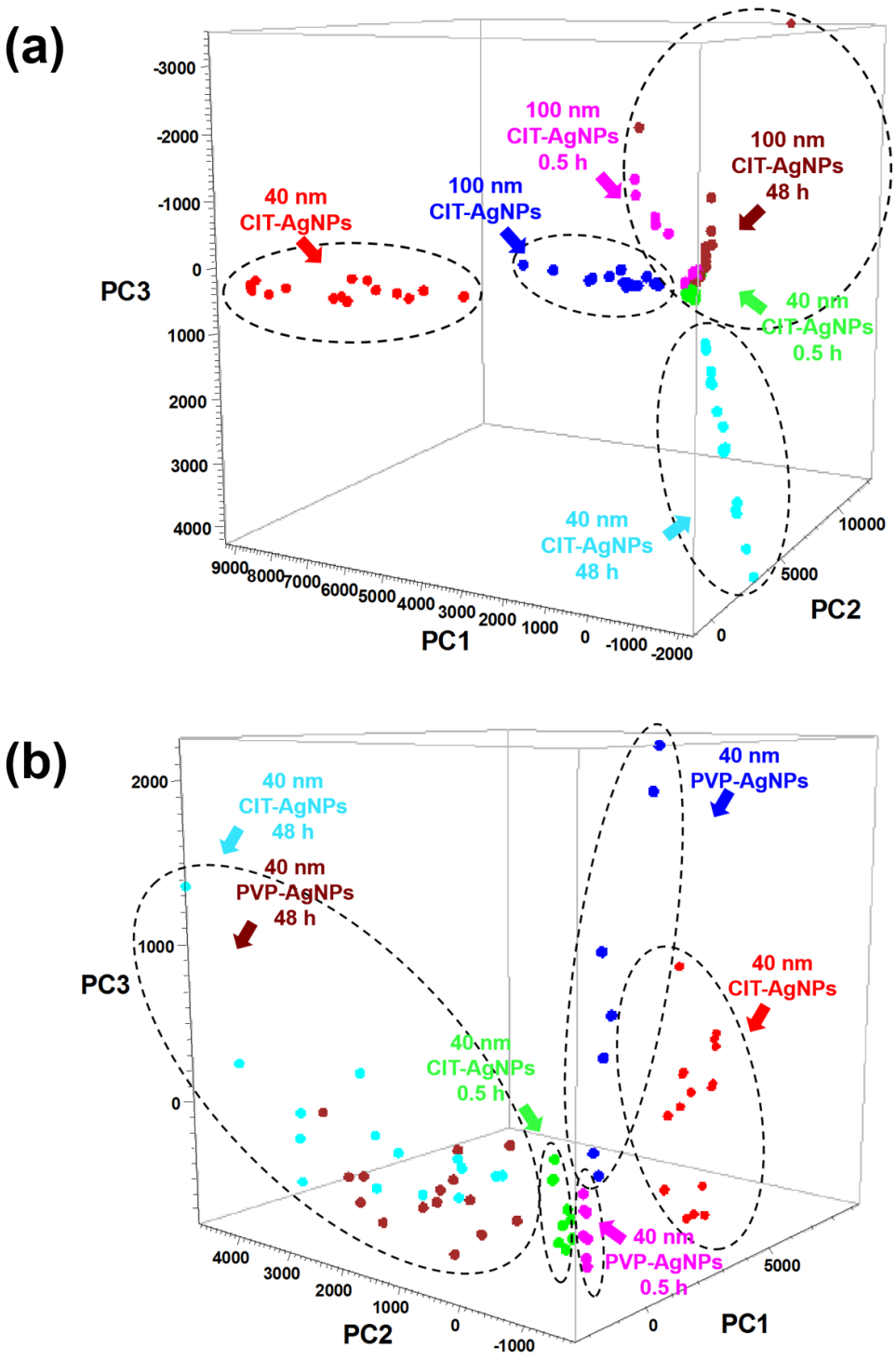

Figure 4. 5 Principal component analysis (PCA) plot of (a) 40 nm CIT- and 100 nm CIT-AgNPs in spinach leaf with different time (0.5 and 48 h), (b) 40 nm CIT- and PVP-AgNP in spinach leaf with different time (0.5 and 48 h).

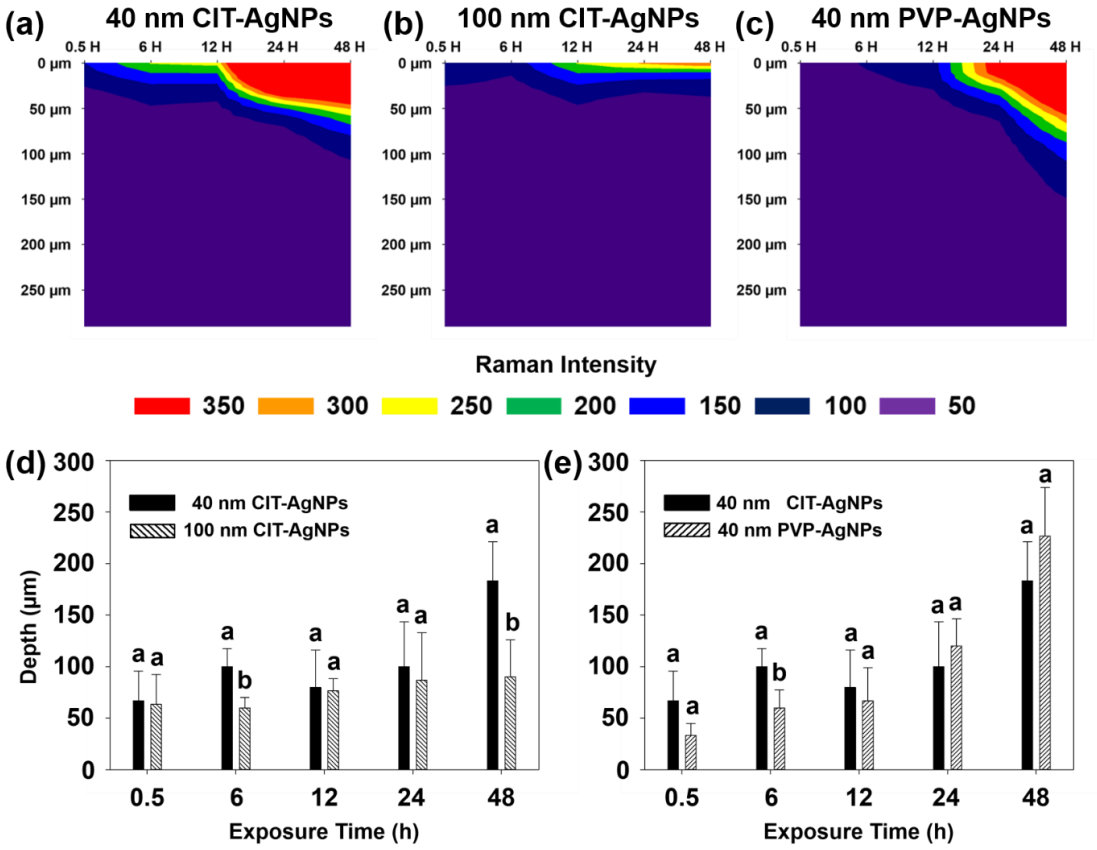

Figure 4. 6 2D SERS depth mapping images of (a) 40 nm CIT-AgNPs, (b) 100 nm CIT-AgNPs, (c) 40 nm PVP-AgNPs penetration following different exposure time based on the highest C-S stretching peaks; (d), (e) Comparison of penetration depth of AgNPs with different sizes (40 and 100 nm) and surface coatings (CIT and PVP) in spinach following different exposure time. Results are expressed as mean value standard deviation (n=3). Different letters represent a significant difference ($P<0.05$).

Figure 4.3a shows the *in situ* SERS spectra of 40 nm CIT-AgNPs in spinach leaf after different exposure time from 0.5 to 48 h. Compared with the spectra of raw spinach leaf and 40 nm CIT-AgNPs, characteristic bands of Cys at position 1033, 955, 735, 680-650 cm^{-1} can be observed from Figure 4.3a after only 0.5 hour. This result indicates a rapid

interaction between 40 nm CIT-AgNPs and Cys in spinach leaf. From the *in vitro* spectra (Figure 4.4), strong C-S band at 658 cm^{-1} also appeared after 0.5 h and the pattern of spectra didn't change from 0.5 to 48 h, demonstrating the rapid interaction between CIT-AgNPs and Cys. Similar result was reported by Gondikas et al., who demonstrated surface ligands (CIT/PVP) on AgNPs could be replaced by Cys after 2 h.[9]> In addition to Cys bands, other SERS bands can also be observed in SERS spectra, which may originate from other bio-components present in spinach leaf, including pectin, lignin, or other polysaccharides.[97] Figure 4.3b shows the *in situ* SERS spectra of 100 nm CIT-AgNPs in spinach leaf after different exposure time from 0.5 to 48 h. Similar to 40 nm CIT-AgNPs, the characteristic bands of Cys, especially at 680-650 cm^{-1}, can be observed, indicating the interaction between 100 nm CIT-AgNPs and induced Cys in spinach leaf. Both Figure 4.3d and 4.3e show that the intensity of C-S band from Cys became stronger with time increasing. This is understandable since the amount of applied AgNPs is specific, while the amount of induced Cys continuously increased from 0.5 to 48 h. These new induced Cys can be further associated with AgNPs and subsequently generate stronger SERS signals. Ma et al. showed that the exposure of engineered *Crambe abyssinica* plants that express the bacterial γ-ECS to AgNPs resulted in a greater cysteine production.[98] Similar result was also reported by Li et al., the overexpression of γ-ECS in *Arabidopsis* contributes to a significant increase in cysteine upon arsenic treatment.[99]

Understanding the biotransformation and determining the distribution of AgNPs in edible plants is very critically important since it controls phytotoxicity and toxicity for consumers. In this study, principal component analysis (PCA) was used to determine the biotransformation of both 40 and 100 nm CIT-AgNPs in spinach leaf. Generally, in the

PCA plot, if the data classes are not overlapping, meaning these classes are significantly different at the p=0.05 level. From Figure 4.5a, the clusters of both *in vitro* 40 and 100 nm CIT-AgNPs (control) are not overlapping. This is reasonable because the SERS intensity of 40 nm CIT-AgNPs is normally stronger than that of 100 nm CIT-AgNPs, which has already been reported by other groups.[10]> However, except the cluster of 40 nm CIT-AgNPs (48 h), the other three clusters, including 40 nm CIT-AgNPs (0.5 h), 100 nm CIT-AgNPs (0.5 h), and 100 nm CIT-AgNPs (48 h), overlapped, indicating no matter what size, CIT-AgNPs experienced similar biotransformation process in spinach leaf. Although clusters of 40 and 100 nm CIT-AgNPs at 48 h did not overlapped, this may be still resulted from the large difference in SERS intensity between 40 and 100 nm CIT-AgNPs.

According to previous study, the penetration of AgNPs into plants is a complex process, depending on many factors (e.g. NP size, surface functionality, chemical composition).[5]> Here, we first compared the penetration ability of AgNPs with different sizes (40 and 100 nm) in spinach leaf. From Figure 4.6a and 4.6d, the penetration depth of 40 nm CIT-AgNPs could reach to 183 ± 38 μm after 48 h. Compared with 40 nm CIT-AgNPs, we found that 100 nm CIT-AgNPs were mostly present closer to the spinach surface (90 ± 36 μm) even after 48 h, indicating the penetration ability of AgNPs is probably size dependent. According to previous study, both pathways (pores of the cuticle and stomata) are more suitable for penetration of NPs with small size, although some other groups found that NPs with large size can enter into plant cells by damage of the cell membrane or by endocytosis.[101] Based on the *in situ* 40 and 100 nm CIT-AgNPs spectra from 0.5 to 48 h we obtained (Figure 4.3a-b), there are no obvious difference. This means the pathway of 40 and 100 nm CIT-AgNPs into spinach leaf may be similar.

4.3.3 Surface Coating Effect on Biotransformation and Penetration Behavior.

Figure 4.3c is the *in situ* SERS spectra of 40 nm PVP-AgNPs in spinach leaf after different exposure time from 0.5 to 48 h. Compared with 40 nm CIT-AgNPs, we note that no new band at 681 cm^{-1} can be observed at 0.5 h, indicating no direct interaction between Cys and 40 nm PVP-AgNPs. This observation could be explained by the fact that the molecular weight of PVP (a long chain polymer with an average molecular weight of 55 000 Da) is much larger than that of CIT (a small amino acid with molecular weight 121 Da), which would compromise the contact between Cys and silver atoms at AgNPs surface. After 6 h, a strong band at around 683 cm^{-1} appeared and became stronger with time increasing (Figure 4.32f). According band assignment, this is still because of the interactions between AgNPs and induced Cys in spinach leaf.

Figure 4.5b is the PCA plot of 40 nm CIT- and PVP-AgNPs in spinach leaf with different time (0.5 and 48 h). As for *in vitro* 40 nm CIT- and PVP-AgNPs (control), their clusters didn't overlap due to their different surface coatings. After 0.5 h, the clusters of 40 nm CIT- and PVP-AgNPs still did not overlap. This is because 40 nm CIT-AgNPs already interacted with Cys produced in spinach leaf at that time while 40 nm PVP-AgNPs didn't, which has been discussed in previous section. However, after 48 h, the clusters of these two kinds of AgNPs overlapped, indicating the insignificant difference between them. According to previous data, we can make a conclusion that no matter what kind of surface coating, AgNPs would end up with AgNPs-Cys in spinach leaf after 48 h.

Figure 4.6c shows the *in situ* 2D SERS penetration images of 40 nm PVP-AgNPs. Similar to both 40 and 100 nm CIT-AgNPs, SERS signals near the surface became stronger with time increasing, which means 40 nm PVP-AgNPs gradually interacts with those

induced Cys in plants. However, we found almost no SERS signals were shown in 0.5 h 2D SERS penetration image. This is because all the 2D SERS penetration images were constructed based on the highest C-S stretching. For 40 nm PVP-AgNPs, no enhanced C-S stretching peak appeared after 0.5 h, thus 2D SERS penetration images cannot truly reflect its real penetration in spinach leaf. Figure 4.6e summarized the penetration behavior of 40 nm PVP-AgNPs in spinach, in which we determined the penetration depth based on the difference of SERS signals between the highest peak in SERS spectra of AgNPs and raw spinach leaf. We found 40 nm PVP-AgNPs gradually penetrated into deeper area with time increasing and reached at 226 ± 47 μm after 48 h ($P < 0.05$). Compared with the penetration profile of 40 nm CIT-AgNPs, the difference between them is not significant. This means surface coating is not a factor that influence the penetration ability of AgNPs in spinach leaf.

4.4 Conclusion

Herein, this study gives insights on *in situ* monitoring the biotransformation and penetration of different kinds of AgNPs in a spinach leaf after foliar exposure. Results show that no matter what kind of sizes (40 and 100 nm) and surface coatings (CIT and PVP), all the AgNPs would interact with Cys and end up with Cys-AgNPs, suggesting a detoxification process in spinach leaf. In addition, the penetration ability of AgNPs depends on NP size rather than surface coating. This type of study shows the promising future of using 2D SERS mapping technique to monitor the biotransformation and distribution of AgNPs in environmental and biological systems. In our future study, additional work will focus on using 2D SERS mapping to monitor the foliar penetration of AgNPs and root uptake of AgNPs over long exposure time in crop plants.

CHAPTER 5

EVALUATION OF POSTHARVEST WASHING ON AGNPS REMOVAL FROM SPINACH LEAVES

5.1 Introduction

The unique antimicrobial and insecticidal properties of silver nanoparticles (AgNPs) have been known for over 100 years and have been adopted commercially across a wide spectrum of agriculture, food, and biomedical applications.[1,5] Since the establishment of US-EPA in 1970, the frequency of EPA-registered silver products has been steadily increasing. EPA-registered AgNPs containing-products can be divided into three categories; (a) AgNPs biocidal additives, (b) Ag-impregnated water filters, and (c) Ag algicides and disinfectants.[1] In recent years, there has been increased interest in the use of inorganic pesticides, such as those containing AgNPs. The manufacturers of these products anticipate that these new pesticides will have greater efficacy in the field, which will subsequently decrease pesticide releases through environmental or "spray" drift and storm water runoff.[3] Currently in the US, approximately 110 AgNPs-containing products had been registered as pesticides by the EPA and several patent applications for AgNPs-based fungicides had been filed.[4,5] The global production of AgNPs was estimated at 500 tons per year and significant increases are anticipated in the future.[6] Previous studies have demonstrated that long term exposure to AgNPs may result in morphologic, physiologic and genetic alternations in plant species and further inhibit crop growth and yield.[49,10]> Importantly, the accumulated AgNPs retained on or in edible plants may transfer through the food chain and pose an unknown risk to human health.[103,104] The toxicity of AgNPs (20 -100 μg mL^{-1}) to human cells, including skin keratinocytes, lung fibroblast cells, and

glioblastoma cells have been demonstrated in several studies.[105,106] Thus, it is important to assess the risk of AgNPs exposure throughout the food chain. An evaluation of the efficacy of different postharvest washing strategies on AgNPs removal that had accumulated on fresh produce surfaces will address some of these critical questions related to exposure.

During the processing of fresh produce, sanitizers are used in postharvest washing to disinfect the process water, effectively inactivating or destroying microorganisms, and preventing cross-contaminations among different batches of food.[6] There are a diverse range of sanitizing agents that have been approved for use of fruits and vegetables; slightly acidified hypochlorite solutions (pH 6.5~7.0) is the most commonly used because of its antimicrobial efficacy and minimal impact on nutritional and flavor quality of the produce.[108,10]> The antimicrobial effects of hypochlorite result from the formation of hypochlorous acid, which is highly reactive with organic nitrogen under aerobic conditions.[110,111] Peroxyacetic acid (CH_3CO_3H) is another widely used sanitizer that has been approved for use on fresh produce by the US Food and Drug Administration (FDA) and US Environmental Protection Agency (EPA).[107] The advantage of peroxyacetic acid over hypochlorite is its stability against influence from organic materials in the washing tank.[112] Importantly, the contact time between both fresh produce and sanitizers is normally less than 5 min and rinsing with potable water is required in the United States.[113–117]

The objective of this study was to evaluate the effectiveness of distilled water and two commonly used sanitizers, Clorox® bleach (contains 8.25% sodium hypochlorite), and Tsunami® 100 (contains 15.2% peroxyacetic acid and 11.2% hydrogen peroxide) at removing surface attached AgNPs from spinach leaves. Since AgNPs are commonly stabilized by sodium citrate, citrate coated AgNPs were selected for this study.[8]> The size

(40 nm) and concentrations (40 mg L^{-1}) of AgNPs used are comparable to those of commercial pesticide products, e.g. CollGen2® (Peschel Instruments Inc, ID) and Colloidal Silver Organic Elemental Biocide (New England Hydroponics, MA). Spinach was chosen because of its large global consumption and high edible tissue surface area, making it an ideal model to study the fate of foliar pesticide residues. Surface enhanced Raman spectroscopy (SERS), scanning electron microscopy (SEM)-energy dispersive spectrometry (EDS), and inductively coupled plasma mass spectrometry (ICP-MS) were used to determine AgNPs removal efficiency. SERS is an effective method for detecting AgNPs after addition of a Raman active ligand that binds strongly to the particles, subsequently yielding a distinct peak for identification and quantification. The enhanced detection mechanism is unique for nano size Ag, effectively discriminating AgNPs from other species.[9] ICP-MS and SEM-EDS were also used to measure the amount of residual total silver and characterize those remaining particles, respectively. This work will help to evaluate the risk level associated with AgNPs contamination in fresh produce, as well as to develop an effective risk mitigation strategy in the future.

5.2 Materials and Methods

5.2.1 Spinach Samples and AgNPs

Organic spinach leaves were purchased from a local grocery store in Amherst, MA and transferred to the Chenoweth Lab at University of Massachusetts Amherst. All spinach leaves were stored at 4 °C and used within 1 day. All leaves were washed with deionized water (Barnstead MicroPure system, Fisher Scientific Co., PA) with a pH of 5.85. AgNPs with an average 40 nm diameter was acquired from NanoComposix (San Diego, CA); The mass concentration (Ag) was 20 mg L^{-1} in citrate solution.

5.2.2 Washing Sanitizer and Washing Conditions

Two commercial produce sanitizer, Clorox® bleach (EPA approved sodium hypochlorite, Reg. No. 5813-100, pH maintained to 6.5-7.5 with acid, CA) and Tsunami® 100 (EPA approved peroxyacetic acid, Reg. No. 1677-164, Ecolab, MN), were used. The main active ingredient of Clorox® bleach is 8.25% sodium hypochlorite (7.85% available chlorine); Tsunami® 100 contains 15.2% peroxyacetic acid and 11.2% hydrogen peroxide. For general produce rinsing operations, 50-200 mg L^{-1} available chlorine for acidified hypochlorite solutions (pH 6.5) or 30-80 mg L^{-1} peroxyacetic acid for Tsunami 100® are commonly used.[112,11]> Here, it should be noted that, although the recommended Clorox® bleach concentration for fresh produce wash is 25 mg L^{-1}, EPA regulatory levels for sodium hypochlorite allow up to 200 mg L^{-1} in direct contact with produce.[114] Thus, in order to maximize the washing effect, 200 mg L^{-1} was selected in our study. In addition, the contact time between fresh produce and the washing sanitizer is typically less than 5 min. In our study, each piece of spinach leaf was contaminated by a drop of 10 µL of 40 nm AgNPs with the concentration of 40 mg L^{-1} and were stored under a fume hood at ambient temperature for 45 min. After drying, the contaminated spinach leaves were immersed into deionized water, 200 mg L^{-1} Clorox® bleach and 80 mg L^{-1} Tsunami® 100 for 5 min, respectively. All leaves were rinsed with deionized water for 1 min to remove sanitizer residue prior to AgNPs analysis. For each treatment, one piece of spinach was used and each treatment was replicated three times. Both raw spinach leaves and AgNPs contaminated leaves without treatment were used as controls.

5.2.3 Recovery of Surface AgNPs Residue for SERS Measurement

Figure 5.1 illustrates the sample collection process from fresh spinach leaves and the principle for AgNPs detection using Scotch double side tape followed by SERS. A Scotch double sided tape (Scotch® Brand, MN) was briefly affixed to the treated spinach leaf surface for 10 s and then immediately removed. This procedure was repeated on the same position three times to ensure total AgNPs removal from the surface, which was verified by optical light microscopy. The double sided tape was then immersed into a 100 mg L^{-1} 4-Mercaptobenzoic acid (Sigma-Aldrich, Missouri, USA) solution for 5 min; this was to ensure complete 4-Mercaptobenzoic acid complexation with AgNPs through Ag-thiol bond formation.[11]> Surface enhanced Raman spectra between 3400 and 400 cm^{-1} were taken by using a DXR Raman spectra-microscope (Thermo Scientific, Madison, WI) under the following conditions: a 20 × confocal microscope objective (3 mm spot diameter and 5 cm^{-1} spectral resolution), 780 nm excitation wavelength, 5 mW laser power and 50 mm slit width for 1 s integration time. Both raw spinach leaves and AgNPs contaminated spinach leaves without treatment were analyzed as controls; $AgNO_3$ and AgCl were used as negative controls.

5.2.4 Scanning Electron Microscopy (SEM)

Treated Spinach leaves (4 cm^2) were freeze-dried (Genesis Pilot Lyophilizer, SP Scientific, NY) overnight and examined by SEM using a FEI Magellan 400 (FEI, OR) with an accelerating voltage of 5 kV under low vacuum conditions. No additional fixative was applied in order to avoid artificial detachment of the AgNPs from the spinach leaves. Both raw spinach leaves and Ag NPs contaminated spinach leaves without treatment were used as controls.

5.2.5 Inductively Coupled Plasma-Mass Spectrometry (ICP-MS)

Ten µL of 40 mg L^{-1} AgNPs treated spinach leaves were dried at ambient temperature, transferred to 15 mL centrifuge tubes and mixed with 3 mL of 68% HNO_3. The samples were subsequently digested at 115 ℃ for 40 min. After cooling, 500 µL of H_2O_2 was added and the samples were incubated at 115 ℃ for 20 min. The digests were diluted 14 fold with deionized water, filtered through Whatman #42 filter paper and analyzed by ICP-MS analysis for total Ag.

5.2.6 Statistical Analysis

Data analysis was performed using OMNIC and TQ Analyst Software (Thermo Fisher Scientific). Data preprocessing algorithms, such as binning, smoothing, and second-derivative transformation, were employed for the spectral data analysis. To determine the influence of washing treatment on AgNPs removal from the leaves, a one-way analysis of variance (ANOVA) followed by a Tukey multiple comparison test was done with SPSS 12.0 software ($P < 0.05$).

5.3 Results

5.3.1 Effectiveness of SERS-Based Method to Detect and Identify AgNPs

Due to its strong binding ability to AgNPs, 4-Mercaptobenzoic acid has been considered as a common SERS indicator and has been widely studied.[119,12]> In a previous study, we used the fungicide ferbam as an indicator molecule but for the current work, there was incompatibility of the adhesive tape with the organic solvent (acetone) used for dissolving the pesticide. 4-Mercaptobenzoic acid can be dissolved in ethanol, which does not react with the adhesive tape. As shown in Figure 5.2, only AgNPs have SERS signals when mixed with 4-Mercaptobenzoic acid. This SERS effect results from localized surface

plasmon resonance (LSPR) and from the chemical enhancement that is produced by the bond between Ag NPs and 4-Mercaptobenzoic acid through the sulfur group (as shown in Figure 5.2).[120] Four distinct Raman peaks of 4-Mercaptobenzoic acid that locate at 1588, 1178, 1130, and 1076 cm^{-1} are consistent with previous reports.[121–123] Among them, the two strong Raman peaks at 1588 and 1076 cm^{-1} can be attributed to the υ(C-C) ring stretching and υ(C-C) ring breathing, respectively. The other two relatively weak Raman peaks at 1130 and 1178 cm^{-1} are attributed to δ(C-H) deformation modes.[121,123,124]

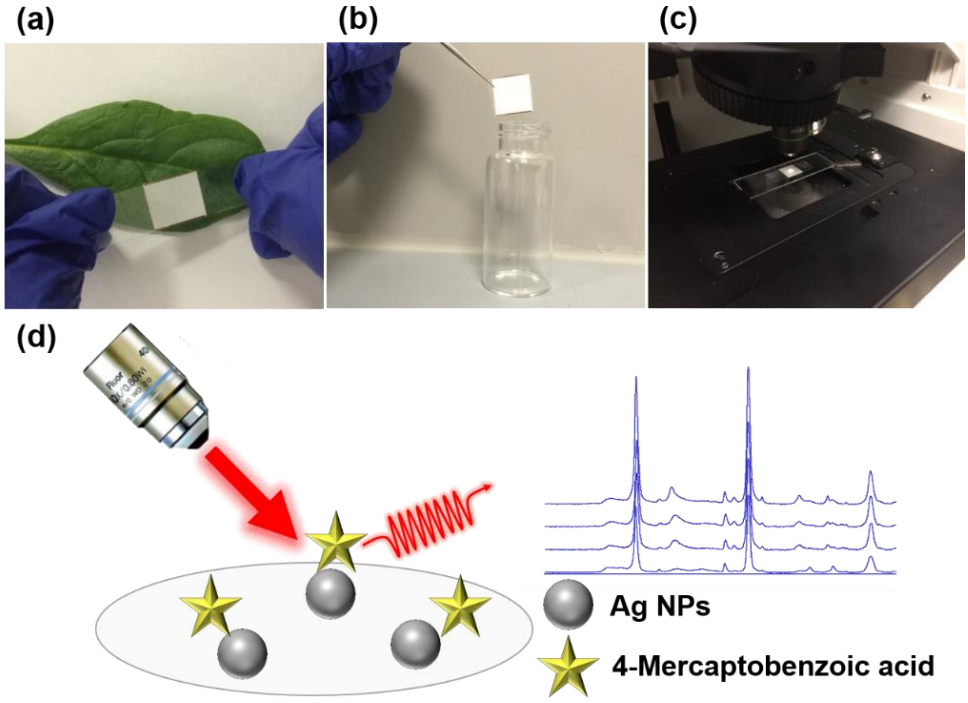

Figure 5. 1 (a) AgNPs collection process from a spinach leaf; (b) Sample mixed with 100 mg L^{-1} 4-Mercaptobenzoic acid; (c) Detection process with the DXR Raman spectrometer; (d) schematic drawing for the detection of AgNPs.

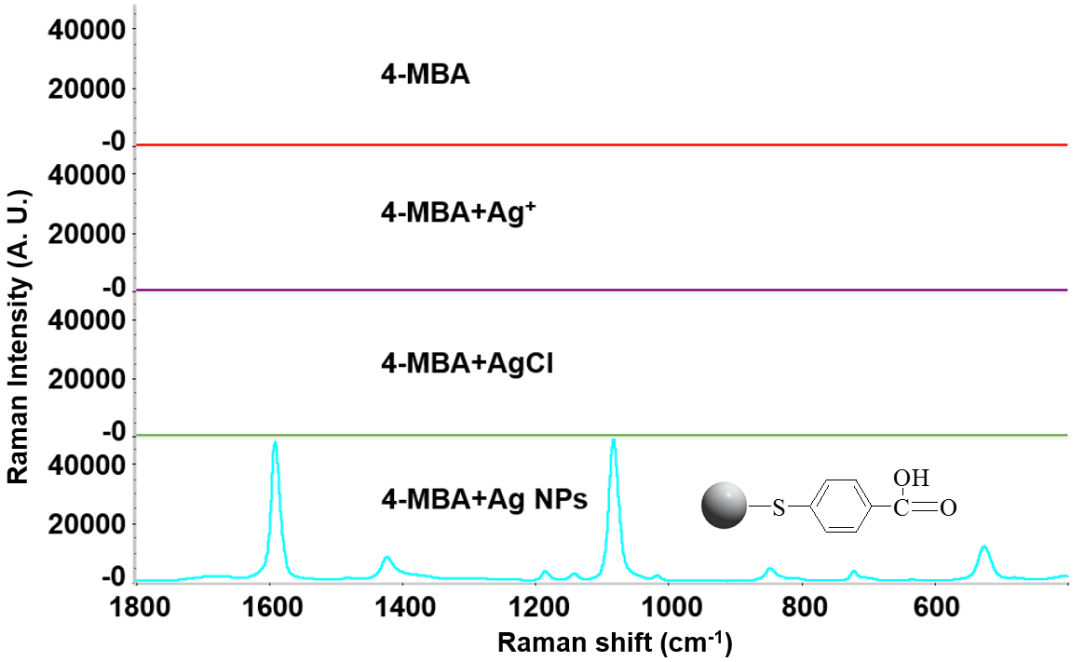

Figure 5. 2 SERS spectra of deionized water (negative control), $AgNO_3$, AgCl, Ag NPs with 100 mg/L 4-Mercaptobenzoic acid.

5.3.2 Standard Curve Establishment for AgNPs Quantification

To accurately quantify the amount of AgNPs on spinach leaves, standard curves were constructed using 10 µL 40 nm AgNPs with different absolute concentrations (0.1, 0.25, 0.5, 1, 5, 10, 20, 40, 60, 100 mg L^{-1}), and deionized water was used as a negative control. As shown in Figure 5.3, no 4-Mercaptobenzoic acid Raman signal was detected for the negative control. The Raman signal intensity was positively correlated with AgNPs concentrations (from 0.1 to 40 mg L^{-1}); this is expected since larger amounts of AgNPs mean the greater available surface area that can be associated with 4-Mercaptobenzoic acid, which subsequently generates the stronger Raman signal. However, when the concentration of applied AgNPs exceeded 40 mg L^{-1}, the net change in Raman intensity decreased, indicating that 0.4 mg L^{-1} is the saturation point. It should be noted that the

correlation coefficients (R^2) between 0.1 - 1 mg L^{-1} and 5 - 40 mg L^{-1} are both greater than 0.97, demonstrating the feasibility of our "tape collection" method for quantitative analysis of AgNPs contaminant residues. Clearly there are additional important factors that need to be considered, such as the size, shape, composition and aggregation status of the NPs. Our current data (Figure 5.3) and that from previous reports demonstrate that SERS intensity is positively correlated with particle size within the 100 nm size range but this gradually decreases beyond 100 nm.[9,10]> In addition, Tiwari et al. reported that among three Ag colloid morphologies (nanospheres, triangular nanprisms and nanorods), Ag nanorods produced the smallest SERS signal whereas the nanoprism exhibits the strongest response.[125] Faulds et al. reported that more enhanced Raman signals would be produced by aggregated nanoparticles as compared with single or small groups of particles.[126] As such, the use of electron microscopy to characterize the physical properties of the particles of interest is clearly important and offers significant advantages for this type of work.

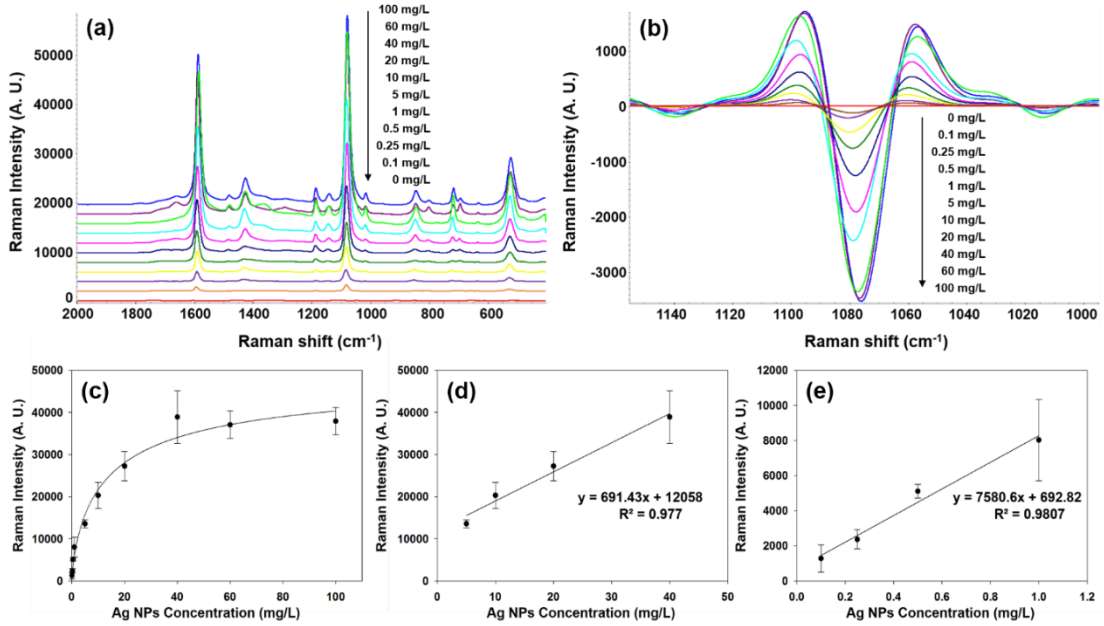

Figure 5. 3 (a) SERS spectra of different concentrations of 40 nm AgNPs with 100 mg L^{-1} 4-Mercaptobenzoic acid; (b) second derivative Raman spectra of the characteristic peak of 4-Mercaptobenzoic acid at 1078 cm^{-1}; (c, d, e) the linear relationship between Raman intensity and AgNPs concentration; The error bars represent the standard errors of three parallel SERS measurements.

5.3.3 Quantification of AgNPs on Leaves after Washing Using SERS

The SERS spectra of AgNPs before and after leaf washing and the corresponding amount of AgNPs quantified are shown in Figure 5.4 and Table 5.1, respectively. The negligible SERS intensity of raw spinach leaves results from the normal Raman signals of 4-Mercaptobenzoic acid. The average intensity SERS response of AgNPs reduced by 12% and 16% after washing by DI water and Tsunami® 100, respectively. However, these decreases were not statistically significantly difference when compared to the control (not washed). The insignificant change demonstrates the low efficacy of these two washing solutions for AgNPs removal. Conversely, the Clorox® bleach treatment resulted in a significant decrease in SERS intensity, equivalent to over a 90% reduction in AgNPs amount. However, the decrease of AgNPs may result from two possible outcomes; a decrease in the total Ag or a transformation of the Ag NPs to other SERS-inactive Ag species.

	Total Ag Measured by ICP-MS	**Total Ag NPs Measured by SERS**	
40 nm Ag NPs Treated Leaf (40 nm, 40×10^{-5} mg)	**Amount of Silver Residue (mg, $\times10^{-5}$)**	**SERS Intensity (A. U.)**	**Corresponding Amount of 40 nm Ag NPs (mg, $\times10^{-5}$)**
Raw Leaf	**1.15 ± 0.01**	**10.77 ± 5.28**	**/**
AgNPs Treated Leaf	**55.31 ± 3.40[b]**	**38928.38 ± 6248.36[b]**	**29.83-47.90**

Deionized Water Wash	**52.62 ± 5.53[b]**	**34293.23 ± 5430.79[b]**	**24.30-40.01**
80 mg/L Tsunami® 100 Wash	**43.80 ± 5.26[a]**	**32789.66 ± 1741.46[b]**	**27.47-32.50**
200 mg/L Clorox® bleach Wash	**49.82 ± 4.00[a]**	**5638.96 ± 2488.26[a]**	**0.32-0.98**

Table 5. 1 Silver amounts on treated and washed spinach using ICP-MS and SERS

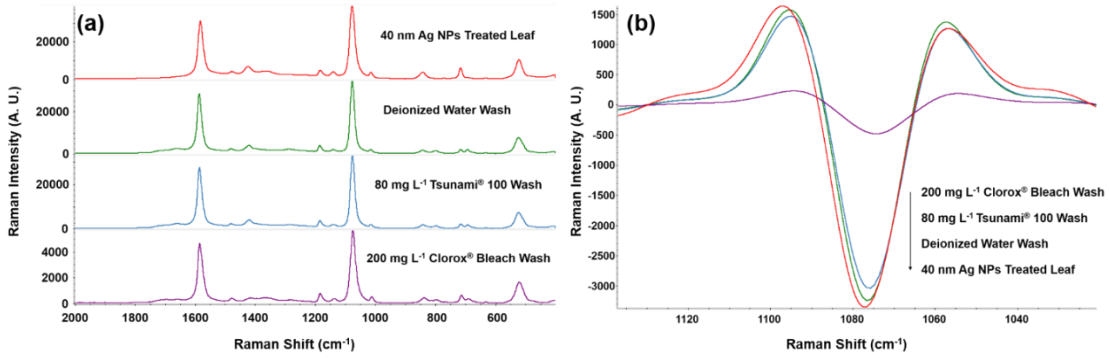

Figure 5. 4 (a) SERS spectra of different washing treatments on 40 nm AgNPs (40 $\times 10^{-5}$ mg) contaminated spinach leaves; (b) second derivative Raman spectra of the characteristic peak of 4-Mercaptobenzoic acid at 1078 cm^{-1}.

5.3.4 Evaluation the Total Ag Removal and Ag species after Washing Using ICP-MS and SEM-EDS

As determined by ICP-MS, the total Ag content does not change after washing with water, but decreases 21% and 10% after washing with Tsunami® 100 and Clorox® bleach, respectively. These findings demonstrate the low efficacy of removing total Ag by the three washing strategies used in the study. SEM images also reveal that the AgNPs can still be clearly seen after washing with DI water and Tsunami® 100 and that the particle size is largely unchanged (Figure 5.6). Interestingly, after washing with Clorox® bleach, both the amount and size of the AgNPs change noticeably. Analysis by EDS confirms that AgNPs

are transformed to AgCl particles with an average size of approximately to 162 ± 51 nm (Figure 5.7).

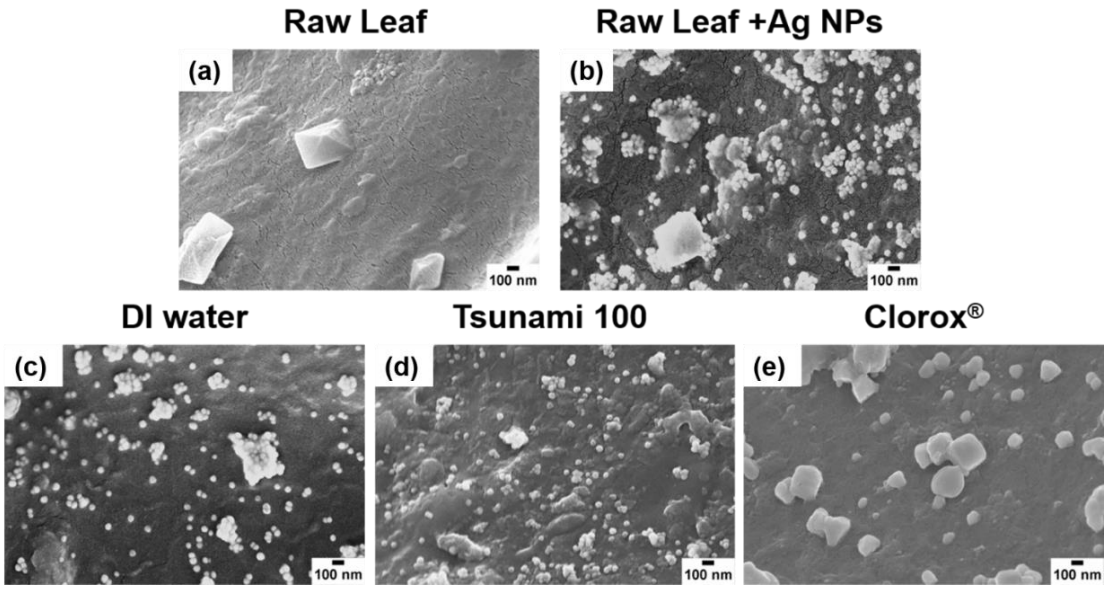

Figure 5. 5 SEM images of spinach leaf surfaces treated with 4×10^{-4} mg AgNPs: (a) raw spinach leaf; (b) AgNPs treated spinach leaves; (c) deionized water washed; (d) 80 mg L^{-1} Tsunami® 100 treated; (e) 200 mg L^{-1} Clorox® bleach solution treated.

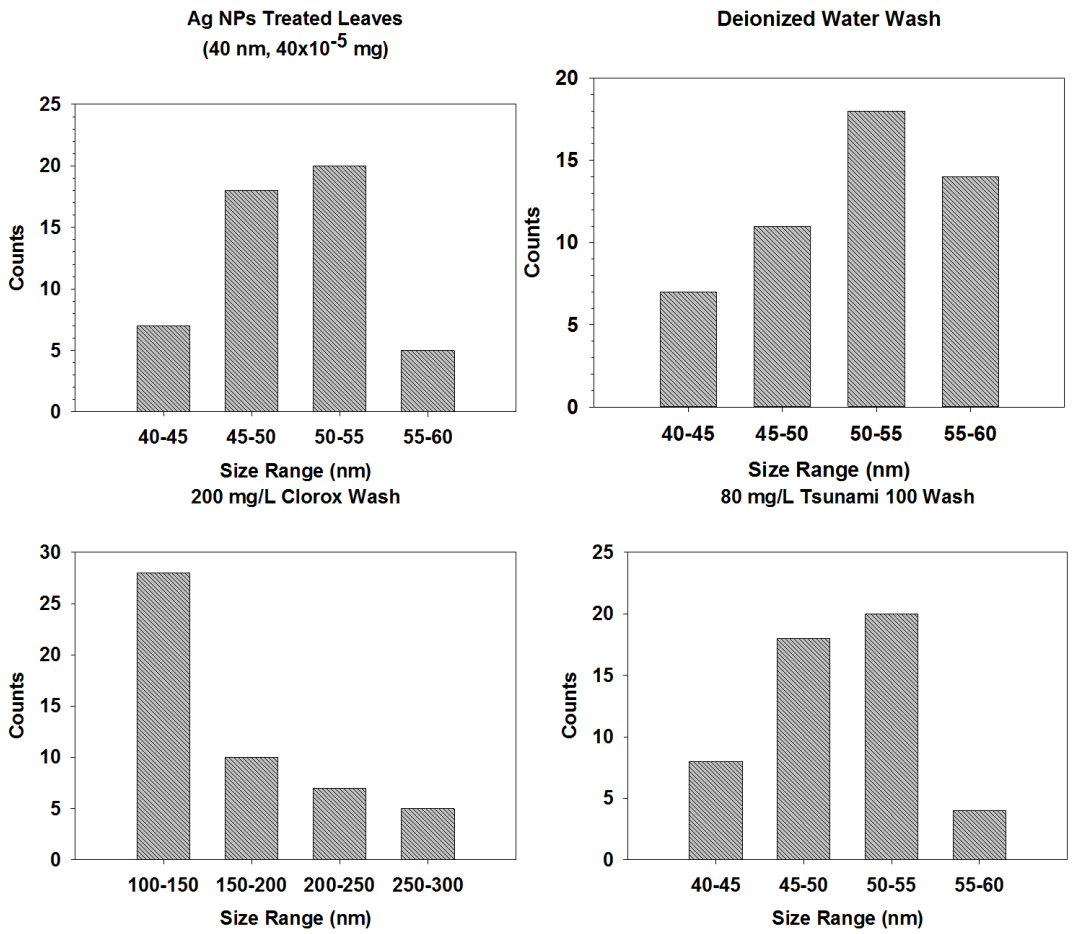

Figure 5. 6 The size distribution of residual particles on spinach after postharvest washing.

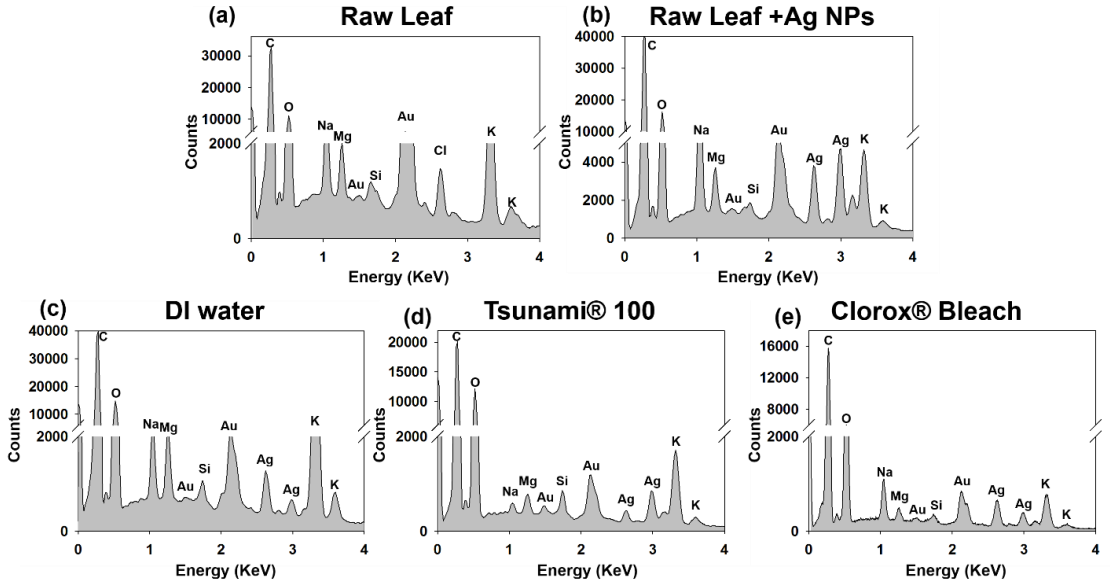

Figure 5. 7 EDS analysis of spinach leaf surfaces treated with 4×10^{-4} mg AgNPs: (a) raw spinach leaf; (b) AgNPs treated spinach leaves; (c) deionized water washed; (d) 80 mg L^{-1} Tsunami® 100 treated; (e) 200 mg L^{-1} Clorox® bleach solution treated.

5.4 Discussion

The findings of this study show that standard washing protocols are insufficient for removing AgNPs, total Ag, or Ag transformed products from food surfaces. An understanding of Ag chemistry in the solutions used will provide clarity to the observed results. It is well known that the oxidation of silver is thermodynamically favored at room temperature ($\Delta G^0_{298} = -11.25$ kJ/mol); thus, metallic silver is generally considered to be sensitive to oxygen.[127–12]> The following reaction stoichiometry was proposed in simple solutions that contain no other oxidants or reductants,

$$\mathbf{2Ag_{(s)} + \frac{1}{2}O_{2(aq)} + 2H^{+}_{(aq)} \Leftrightarrow 2Ag^{+}_{(aq)} + H_2O_{(l)}}$$

Previous studies have shown that DI water can be used to remove alumina NPs that had been applied to tomato surfaces but not for titanium and silica NPs on that same fruit.[13]> The authors postulated that the large difference (4 or more pH units) between the pH of the washing solution and the NPs isoelectric point (IEP) increase the zeta potential while decreasing the hydrodynamic size, thereby enhancing particle removal. Here the difference (3.65 units) between pH of our DI water (pH ≈5.85) and the IEP of AgNPs (IEP $_{AgNPs}$ ≈ 2.2) may explain the low washing efficiency. In addition, since AgNPs are more easily to form a strong binding with those biomolecules with thiol group in plants, which may reduce the removal efficiency as well.[51] Our results are in agree with Laure et al study,[51] in which they demonstrated that the classical washing process could only remove those bigger Ag agglomerates from the surface of lettuce and did not result a significant decrease in the total amount of Ag.

In the Tsunami® 100 solution, the pH is 3.6 and the main active agents are peroxyacetic acid and hydrogen peroxide. In addition, metallic silver can be oxidized by H_2O_2 and peroxyacetic acid in a similar way since the acid will break down in to acetic acid and hydrogen peroxide. [13]> The hydrogen peroxide will react with metallic silver to release Ag^+ with simultaneous formation of the hydroxyl radical,[132]

$$\mathbf{Ag_{(s)} + H_2O_2 \longrightarrow Ag^{+}_{(aq)} + OH^{\cdot} + OH^{-}}$$

Then, the hydroxyl radical can further oxidize metallic silver,[13]>

$$\mathbf{Ag_{(s)} + OH^{\cdot} \longrightarrow Ag^{+}_{(aq)} + OH^{-}}$$

However, it is obvious that Tsunami® 100 solution was still ineffective at removing total Ag and AgNPs. This may due to the fact that difference between the pH and IEP$_{AgNPs}$

is still smaller than 4 units, which decreases Ag NPs removal. In addition, insufficient contact time and/or concentration for the washing protocol used may also be the reasons.

For the Clorox® bleach solution (pH ≈ 6.5), the difference between the pH and IEP_{AgNPs} is larger than 4 units, which should facilitate AgNPs removal. In addition, the main oxidant in Clorox® bleach solution is sodium hypochlorite that will readily transform metallic silver to Ag^+. In fact, most of AgNPs will be quickly oxidized by sodium hypochlorite due to its strong oxidizing ability. Hypochlorous acid would form first and then partially release hypochlorite ion (pKa=7.4) upon dissolution in water. Partial hypochlorite ions would further dissociate into chloride ion.[13]> We propose that relatively small amounts of Cl^- anions scavenge Ag^+ and then form AgCl precipitants;[135]

$$\mathbf{Ag^+ + Cl^- \longrightarrow AgCl}$$

Impellitteri et al. found similar transformation from AgNPs to AgCl when they attempted to identify the speciation of AgNPs in antimicrobial fabric after hypochlorite/detergent solution exposure.[13]> Importantly, AgCl may still pose a risk to humans; the toxicity of AgNPs, AgCl and Ag ions has been reviewed in recent years[136–138]. For example, Choi et al. showed that AgCl colloids are as effective as Ag ions at inhibiting the growth of nitrifying bacteria but are less effective than AgNPs.[136] However, comparisons to AgNPs cannot be generalized since the toxicity is strongly particle size dependent.[139]

Herein, we evaluated the postharvest washing efficiency of several treatments, including deionized water, Tsunami® 100 and Clorox® bleach, on AgNPs removal from spinach leaves. Large amounts of AgNPs residues were still present on the leaf surface after rinsing with deionized water. The oxidizing agents of Tsunami® 100 (80 mg L^{-1}) and

Clorox® bleach (200 mg L^{-1}) partly oxidized AgNPs and subsequently released Ag^{+} ions. This resulted in reductions in AgNPs presence; 16% for Tsunami® (although not statistically significant) but nearly 90% for Clorox® with SERS analysis. However, with regard to total Ag presence as measured by ICP-MS, there was no obvious difference between the two treatments. This can be explained by the fact that released Ag^{+} ions reacted with free chloride anions in Clorox® bleach and resulted in the formation AgCl particles (average size 162 ± 51 nm) on the spinach leaves. Due to the fact that AgCl is still potentially toxic to humans, as well as still having the potential to be further oxidized to ions or reduced to NP form, a significant safety concern remains. Future research will focus on the development of a safe, effective, and practice washing protocol for removing AgNPs from fresh produce surfaces. Additional work will address the issue of AgNPs penetration, and potential methods to alleviate the NP content under these circumstances.

CHAPTER 6

CONCLUDING REMARKS

In summary, in the first part, the capacity of SERS to detect AuNPs and to characterize the interactions between AuNPs and biomolecules in plants was evaluated. Our results showed that SERS could be used to detect AuNPs with size range from 15 to 125 nm. Through in vivo SERS mapping, the distribution of AuNPs on and in spinach leaf could be monitored by the SERS images collected from biomolecules attached to the nanoparticles. More importantly, the interactions between AuNPs and biomolecules (e.g. chlorophylls, carotenoids) could be determined through analyzing the enhanced Raman signatures of biomolecules of the spinach, which facilitates our understanding of how AuNPs attach on and penetrate into spinach leaf. TEM-EDS was used to visualize the presence of AuNPs in chloroplasts of spinach leaf and validate our SERS results. In the second part, due to the increasing commercialization of AgNPs in agricultural applications, such as biocides, SERS mapping was used to *in situ* and real time investigate the interactions between spinach leaf and AgNPs with different surface coatings/sizes. Our results showed that no matter what kind of sizes (40 and 100 nm) and surface coatings (CIT and PVP), all the AgNPs would interact with Cys and end up with Cys-AgNPs, suggesting a detoxification process in spinach leaf. We concluded that the surface coating mainly affects the initial speed of interaction while the size of AgNPs is the main factor that affects the penetration depth. In the third part, the postharvest washing efficiency of DI water and two common sanitizers (Clorox® bleach and Tsunami® 100) on AgNPs removal was evaluated by a SERS, ICP-MS, and SEM-EDS. Through analyzing the obtained data, we found that, both DI water and Tsunami® 100 could not effectively decrease the amount of

surface attached AgNPs, indicating the low efficiency of these two methods on AgNPs removal. For Clorox® bleach, although the amount of AgNPs significantly decreased, parts of these AgNPs were transformed into AgCl. Since the fact that AgCl is still potentially toxic to humans, as well as still having the potential to be further oxidized to ions or reduced to NP form, a significant safety concern remains.

Through this study, we have a better understanding of how AgNPs would possibly contaminate fresh produce, such as spinach, how they attach onto and internalize into the spinach leaf, how they distribute and transform, as well as whether common washing sanitizers can remove AgNPs on spinach leaf or not. Understanding these processes will help us to evaluate the risk level of the AgNPs contamination in fresh produce and develop a better control strategy to prevent contamination, which is important to maintain the safety and sustainability of agriculture and food system. In our future study, we will use 2D SERS mapping technique to identify, quantify and characterize AgNPs distribution in plant tissues and their fate via root-to-shoot exposure. In addition, more effective washing method will also be developed in the following study.

BIBLIOGRAPHY

(1) Nowack, B.; Krug, H. F.; Height, M. 120 years of nanosilver history: Implications for policy makers. *Environ. Sci. Technol.* **2011**, *45* (4), 1177–1183.

(2) Sharma, V. K.; Siskova, K. M.; Zboril, R.; Gardea-Torresdey, J. L. Organic-coated silver nanoparticles in biological and environmental conditions: Fate, stability and toxicity. *Adv. Colloid Interface Sci.* **2014**, *204*, 15–34.

(3) Zhang, Z.; Kong, F.; Vardhanabhuti, B.; Mustapha, A.; Lin, M. Detection of engineered silver nanoparticle contamination in pears. *J. Agric. Food Chem.* **2012**, *60* (43), 10762–10767.

(4) Bergeson, L. L. Nanosilver Pesticide Products: What Does the Future Hold? *Environ. Qual. Manag.* **2010**, *19* (4), 73–82.

(5) Gogos, A.; Knauer, K.; Bucheli, T. D. Nanomaterials in plant protection and fertilization: Current state, foreseen applications, and research priorities. *J. Agric. Food Chem.* **2012**, *60* (39), 9781–9792.

(6) Mueller, N. C.; Nowack, B. Exposure modeling of engineered nanoparticles in the environment. *Environ. Sci. Technol.* **2008**, *42* (12), 4447–4453.

(7) Eom, H.-J.; Choi, J. p38 MAPK activation, DNA damage, cell cycle arrest and apoptosis as mechanisms of toxicity of silver nanoparticles in Jurkat T cells. *Environ. Sci. Technol.* **2010**, *44* (21), 8337–8342.

(8) Tiede, K.; Boxall, A. B. a; Tear, S. P.; Lewis, J.; David, H.; Hassellov, M. Detection and characterization of engineered nanoparticles in food and the environment. *Food Addit. Contam. Part A. Chem. Anal. Control. Expo. Risk Assess.* **2008**, *25* (7), 795–821.

(9) Guo, H.; Zhang, Z.; Xing, B.; Mukherjee, A.; Musante, C.; White, J. C.; He, L. Analysis of Silver Nanoparticles in Antimicrobial Products Using Surface-Enhanced Raman Spectroscopy (SERS). *Environ. Sci. Technol.* **2015**, *49* (7), 4317–4324.

(10) Culha, M.; Cullum, B.; Lavrik, N.; Klutse, C. K. Surface-enhanced Raman scattering as an emerging characterization and detection technique. *J. Nanotechnol.* **2012**, *2012*.

(11) Haynes, C. L.; McFarland, A. D.; Van Duyne, R. P. Surface-enhanced Raman spectroscopy. *Anal. Chem.* **2005**, *77* (17), 338 A – 346 A.

(12) Fan, M.; Andrade, G. F. S.; Brolo, A. G. A review on the fabrication of substrates for surface enhanced Raman spectroscopy and their applications in analytical chemistry. *Anal. Chim. Acta* **2011**, *693* (1), 7–25.

(13) Kim, K.; Shin, K. S. Surface-enhanced Raman scattering: a powerful tool for chemical identification. *Anal. Sci.* **2011**, *27* (8), 775.

(14) Willets, K. A. Surface-enhanced Raman scattering (SERS) for probing internal cellular structure and dynamics. *Anal. Bioanal. Chem.* **2009**, *394* (1), 85–94.

(15) Xie, W.; Su, L.; Shen, A.; Materny, A.; Hu, J. Application of surface-enhanced Raman scattering in cell analysis. *J. Raman Spectrosc.* **2011**, *42* (6), 1248–1254.

(16) Wang, Y.; Yan, B.; Chen, L. SERS tags: novel optical nanoprobes for bioanalysis. *Chem. Rev.* **2012**, *113* (3), 1391–1428.

(17) Vo-Dinh, T.; Yan, F.; Wabuyele, M. B. Surface-enhanced Raman scattering for biomedical diagnostics and molecular imaging. In *Surface-Enhanced Raman Scattering*; Springer, 2006; pp 409–426.

(18) Xie, W.; Schlücker, S. Medical applications of surface-enhanced Raman scattering. *Phys. Chem. Chem. Phys.* **2013**, *15* (15), 5329–5344.

(19) Efrima, S.; Zeiri, L. Understanding SERS of bacteria. *J. Raman Spectrosc.* **2009**, *40* (3), 277–288.

(20) Craig, A. P.; Franca, A. S.; Irudayaraj, J. Surface-enhanced Raman spectroscopy applied to food safety. *Annu. Rev. Food Sci. Technol.* **2013**, *4*, 369–380.

(21) Zheng, J.; He, L. Surface-Enhanced Raman Spectroscopy for the Chemical Analysis of Food. *Compr. Rev. food Sci. food Saf.* **2014**, *13* (3), 317–328.

(22) Li, D.-W.; Zhai, W.-L.; Li, Y.-T.; Long, Y.-T. Recent progress in surface enhanced Raman spectroscopy for the detection of environmental pollutants. *Microchim. Acta* **2013**, *181* (1-2), 23–43.

(23) Halvorson, R. A.; Vikesland, P. J. Surface-enhanced Raman spectroscopy (SERS) for environmental analyses. *Environ. Sci. Technol.* **2010**, *44* (20), 7749–7755.

(24) Ahamed, M.; AlSalhi, M. S.; Siddiqui, M. K. J. Silver nanoparticle applications and human health. *Clin. Chim. Acta* **2010**, *411* (23-24), 1841–1848.

(25) Lea, M. C. Allotropic forms of silver. *Am. J. Sci.* **1889**, No. 222, 476–491.

(26) Frens, G.; Overbeek, J. T. G. Carey Lea's colloidal silver. *Kolloid-Zeitschrift und Zeitschrift für Polym.* **1969**, *233* (1-2), 922–929.

(27) Boese, K. Über Collargol, seine Anwendung und seine Erfolge in der Chirurgie und Gynäkologie. *Langenbeck's Arch. Surg.* **1921**, *163* (1), 62–84.

(28) Fung, M. C.; Bowen, D. L. Silver products for medical indications: risk-benefit assessment. *J. Toxicol. Clin. Toxicol.* **1996**, *34* (1), 119–126.

(29) Kim, H. S.; Kang, H. S.; Chu, G. J.; Byun, H. S. Antifungal effectiveness of nanosilver colloid against rose powdery mildew in greenhouses. In *Solid State Phenomena*; Trans Tech Publ, 2008; Vol. 135, pp 15–18.

(30) Alavi, S. V; Dehpour, A. A. Evaluation of the nanosilver colloidal solution in comparison with the registered fungicide to control greenhouse cucumber downy mildew disease in the north of Iran. In *VI International Postharvest Symposium 877*; 2009; pp 1643–1646.

(31) Judy, J. D.; Unrine, J. M.; Bertsch, P. M. Evidence for biomagnification of gold nanoparticles within a terrestrial food chain. *Environ. Sci. Technol.* **2011**, *45* (2), 776–781.

(32) Judy, J. D.; Unrine, J. M.; Rao, W.; Bertsch, P. M. Bioaccumulation of gold nanomaterials by Manduca sexta through dietary uptake of surface contaminated plant tissue. *Environ. Sci. Technol.* **2012**, *46* (22), 12672–12678.

(33) Nel, A.; Xia, T.; Mädler, L.; Li, N. Toxic potential of materials at the nanolevel. *Science (80-.).* **2006**, *311* (5761), 622–627.

(34) Ryter, S. W.; Kim, H. P.; Hoetzel, A.; Park, J. W.; Nakahira, K.; Wang, X.; Choi, A. M. K. Mechanisms of cell death in oxidative stress. *Antioxid. Redox Signal.* **2007**, *9* (1), 49–89.

(35) Ahamed, M.; Siddiqui, M. A.; Akhtar, M. J.; Ahmad, I.; Pant, A. B.; Alhadlaq, H. A. Genotoxic potential of copper oxide nanoparticles in human lung epithelial cells. *Biochem. Biophys. Res. Commun.* **2010**, *396* (2), 578–583.

(36) Kim, Y. S.; Kim, J. S.; Cho, H. S.; Rha, D. S.; Kim, J. M.; Park, J. D.; Choi, B. S.; Lim, R.; Chang, H. K.; Chung, Y. H. Twenty-eight-day oral toxicity, genotoxicity, and gender-related tissue distribution of silver nanoparticles in Sprague-Dawley rats. *Inhal. Toxicol.* **2008**, *20* (6), 575–583.

(37) Cha, K.; Hong, H.-W.; Choi, Y.-G.; Lee, M. J.; Park, J. H.; Chae, H.-K.; Ryu, G.; Myung, H. Comparison of acute responses of mice livers to short-term exposure to nano-sized or micro-sized silver particles. *Biotechnol. Lett.* **2008**, *30* (11), 1893–1899.

(38) Mavrocordatos, D.; Perret, D.; Leppard, G. G. Strategies and advances in the characterisation of environmental colloids by electron microscopy. *IUPAC Ser. Anal. Phys. Chem. Environ. Syst.* **2007**, *10*, 345.

(39) Majumdar, S.; Peralta-Videa, J. R.; Bandyopadhyay, S.; Castillo-Michel, H.; Hernandez-Viezcas, J. A.; Sahi, S.; Gardea-Torresdey, J. L. Exposure of cerium oxide nanoparticles to kidney bean shows disturbance in the plant defense mechanisms. *J. Hazard. Mater.* **2014**, *278*, 279–287.

(40) Sur, U. K.; Sung, S. H.; Stiles, P. L.; Dieringer, J. a; Shah, N. C.; Van Duyne, R. P. Surface-enhanced Raman spectroscopy. *Annu. Rev. Anal. Chem. (Palo Alto. Calif).* **2008**, *1* (February), 601–626.

(41) McCreery, R. L. *Raman spectroscopy for chemical analysis*; John Wiley & Sons, 2005; Vol. 225.

(42) Zeiri, L. SERS of plant material. *J. Raman Spectrosc.* **2007**, *38* (7), 950–955.

(43) Espina Palanco, M.; Mogensen, K. B.; Kneipp, K. Raman spectroscopic probing of plant material using SERS. *J. Raman Spectrosc.* **2015**.

(44) Shen, A.; Guo, J.; Xie, W.; Sun, M.; Richards, R.; Hu, J. Surface-enhanced Raman spectroscopy in living plant using triplex Au Ag C core–shell nanoparticles. *J. Raman Spectrosc.* **2011**, *42* (4), 879–884.

(45) Hou, R.; Pang, S.; He, L. In situ SERS detection of multi-class insecticides on plant surfaces. *Anal. Methods* **2015**, *7* (15), 6325–6330.

(46) Yang, T.; Zhang, Z.; Zhao, B.; Hou, R.-Y.; Kinchla, A.; Clark, J. M.; He, L. Real-time and in situ monitoring of pesticide penetration in edible leaves by surface-enhanced Raman scattering mapping. *Environ. Sci. Technol.* **2016**, *50*, 3937–3944.

(47) Whitacre, D. M.; Gunther, F. A. *Reviews of environmental contamination and toxicology*; Springer: New York, 2012.

(48) Remédios, C.; Rosário, F.; Bastos, V. Environmental Nanoparticles Interactions with Plants: Morphological, Physiological, and Genotoxic Aspects. *J. Bot.* **2012**, *2012*, 1–8.

(49) Rico, C. M.; Majumdar, S.; Duarte-Gardea, M.; Peralta-Videa, J. R.; Gardea-Torresdey, J. L. Interaction of nanoparticles with edible plants and their possible implications in the food chain. *J. Agric. Food Chem.* **2011**, *59* (8), 3485–3498.

(50) Hong, J.; Peralta-Videa, J. R.; Rico, C.; Sahi, S.; Viveros, M. N.; Bartonjo, J.; Zhao, L.; Gardea-Torresdey, J. L. Evidence of translocation and physiological impacts of foliar applied CeO2 nanoparticles on cucumber (Cucumis sativus) plants. *Environ. Sci. Technol.* **2014**, *48* (8), 4376–4385.

(51) Larue, C.; Castillo-Michel, H.; Sobanska, S.; Cécillon, L.; Bureau, S.; Barthès, V.; Ouerdane, L.; Carrière, M.; Sarret, G. Foliar exposure of the crop Lactuca sativa to silver nanoparticles: Evidence for internalization and changes in Ag speciation. *J. Hazard. Mater.* **2014**, *264*, 98–106.

(52) Larue, C.; Castillo-Michel, H.; Sobanska, S.; Trcera, N.; Sorieul, S.; Cécillon, L.; Ouerdane, L.; Legros, S.; Sarret, G. Fate of pristine TiO2 nanoparticles and aged paint-containing TiO2 nanoparticles in lettuce crop after foliar exposure. *J. Hazard. Mater.* **2014**, *273*, 17–26.

(53) Gardea-Torresdey, J. L.; Rico, C. M.; White, J. C. Trophic transfer, transformation, and impact of engineered nanomaterials in terrestrial environments. *Environ. Sci. Technol.* **2014**, *48* (5), 2526–2540.

(54) Servin, A. D.; Morales, M. I.; Castillo-Michel, H.; Hernandez-Viezcas, J. A.; Munoz, B.; Zhao, L.; Nunez, J. E.; Peralta-Videa, J. R.; Gardea-Torresdey, J. L. Synchrotron verification of TiO2 accumulation in cucumber fruit: A possible pathway of TiO2 nanoparticle transfer from soil into the food chain. *Environ. Sci. Technol.* **2013**, *47* (20), 11592–11598.

(55) Darlington, T. K.; Neigh, A. M.; Spencer, M. T.; Nguyen, O. T.; Oldenburg, S. J. Nanoparticle characteristics affecting environmental fate and transport through soil. *Environ. Toxicol. Chem.* **2009**, *28* (6), 1191–1199.

(56) Bozich, J. S.; Lohse, S. E.; Torelli, M. D.; Murphy, C. J.; Hamers, R. J.; Klaper, R. D. Surface chemistry, charge and ligand type impact the toxicity of gold nanoparticles to Daphnia magna. *Environ. Sci. Nano* **2014**, *1* (3), 260–270.

(57) Judy, J. D.; Unrine, J. M.; Rao, W.; Wirick, S.; Bertsch, P. M. Bioavailability of gold nanomaterials to plants: importance of particle size and surface coating. *Environ. Sci. Technol.* **2012**, *46* (15), 8467–8474.

(58) Zhu, Z.-J.; Wang, H.; Yan, B.; Zheng, H.; Jiang, Y.; Miranda, O. R.; Rotello, V. M.; Xing, B.; Vachet, R. W. Effect of surface charge on the uptake and distribution of gold nanoparticles in four plant species. *Environ. Sci. Technol.* **2012**, *46*, 12391–12398.

(59) López-Moreno, M. L.; De La Rosa, G.; Hernández-Viezcas, J. a.; Peralta-Videa, J. R.; Gardea-Torresdey, J. L. X-ray absorption spectroscopy (XAS) corroboration of the uptake and storage of ceo2 nanoparticles and assessment of their differential toxicity in four edible plant species. *J. Agric. Food Chem.* **2010**, *58* (6), 3689–3693.

(60) Uzu, G.; Sobanska, S.; Sarret, G.; Muñoz, M.; Dumat, C. Foliar Lead uptake by lettuce exposed to atmospheric fallouts. *Environ. Sci. Technol.* **2010**, *44* (3), 1036–1042.

(61) Kurepa, J.; Paunesku, T.; Vogt, S.; Arora, H.; Rabatic, B. M.; Lu, J.; Wanzer, M. B.; Woloschak, G. E.; Smalle, J. a. Uptake and distribution of ultrasmall anatase TiO2 alizarin red s nanoconjugates in arabidopsis thaliana. *Nano Lett.* **2010**, *10* (7), 2296–2302.

(62) Gui, X.; He, X.; Ma, Y.; Zhang, P.; Li, Y.; Ding, Y.; Yang, K.; Li, H.; Rui, Y.; Chai, Z.; et al. Quantifying the distribution of ceria nanoparticles in cucumber roots: the influence of labeling. *RSC Adv.* **2015**, *5* (6), 4554–4560.

(63) Punshon, T.; Guerinot, M. Lou; Lanzirotti, A. Using synchrotron X-ray fluorescence microprobes in the study of metal homeostasis in plants. *Ann. Bot.* **2009**, *103* (5), 665–672.

(64) Vo-Dinh, T.; Yan, F.; Wabuyele, M. B. Surface-enhanced Raman scattering for medical diagnostics and biological imaging. *J. raman Spectrosc.* **2005**, *36* (6-7), 640–647.

(65) Craig, A. P.; Franca, A. S.; Irudayaraj, J. Surface-Enhanced Raman Spectroscopy Applied to Food Safety. *Annu. Rev. Food Sci. Technol.* **2013**, *4* (1), 369–380.

(66) Rodríguez-Lorenzo, L.; Krpetic, Z.; Barbosa, S.; Alvarez-Puebla, R. A.; Liz-Marzán, L. M.; Prior, I. A.; Brust, M. Intracellular mapping with SERS-encoded gold nanostars. *Integr. Biol.* **2011**, *3* (9), 922–926.

(67) Ando, J.; Fujita, K.; Smith, N. I.; Kawata, S. Dynamic SERS imaging of cellular transport pathways with endocytosed gold nanoparticles. *Nano Lett.* **2011**, *11* (12), 5344–5348.

(68) Walkey, C. D.; Olsen, J. B.; Guo, H.; Emili, A.; Chan, W. C. W. Nanoparticle size and surface chemistry determine serum protein adsorption and macrophage uptake. *J. Am. Chem. Soc.* **2012**, *134* (4), 2139–2147.

(69) Bozzola, J. J.; Russell, L. D. *Electron microscopy: principles and techniques for biologists*; Jones & Bartlett Learning: Burlington, 1999.

(70) Eustis, S.; el-Sayed, M. a. Why gold nanoparticles are more precious than pretty gold: noble metal surface plasmon resonance and its enhancement of the radiative and nonradiative properties of nanocrystals of different shapes. *Chem. Soc. Rev.* **2006**, *35* (3), 209–217.

(71) Schulz, H.; Baranska, M. Identification and quantification of valuable plant substances by IR and Raman spectroscopy. *Vib. Spectrosc.* **2007**, *43* (1), 13–25.

(72) Withnall, R.; Chowdhry, B. Z.; Silver, J.; Edwards, H. G. M.; de Oliveira, L. F. C. Raman spectra of carotenoids in natural products. *Spectrochim. Acta Part A Mol. Biomol. Spectrosc.* **2003**, *59* (10), 2207–2212.

(73) Schwartzberg, A. M.; Grant, C. D.; Wolcott, A.; Talley, C. E.; Huser, T. R.; Bogomolni, R.; Zhang, J. Z. Unique gold nanoparticle aggregates as a highly active surface-enhanced raman scattering substrate. *J. Phys. Chem. B* **2004**, *108* (50), 19191–19197.

(74) Laing, S.; Gracie, K.; Faulds, K. Multiplex in vitro detection using SERS. *Chem. Soc. Rev.* **2016**, *45*, 1901–1918.

(75) Barazzouk, S.; Kamat, P. V; Hotchandani, S. Photoinduced electron transfer between chlorophyll a and gold nanoparticles. *J. Phys. Chem. B* **2005**, *109*, 716–723.

(76) Barazzouk, S.; Bekalé, L.; Hotchandani, S. Enhanced photostability of chlorophyll-a using gold nanoparticles as an efficient photoprotector. *J. Mater. Chem.* **2012**, *22* (48), 25316–25324.

(77) Kidmose, U.; Edelenbos, M.; Christensen, L. P.; Hegelund, E. Chromatographic determination of changes in pigments in spinach (Spinacia oleracea L.) during processing. *J. Chromatogr. Sci.* **2005**, *43* (October), 466–472.

(78) Pavia, D.L., Lampman, G.M., Kriz, G.S., and Engel, R. . Isolation of Chlorophyll and Carotenoid Pigments from Spinach. *Introd. to Org. Lab. Tech. A Microscale Approach 3rd Ed.* **1999**, 1–7.

(79) Amiard, V.; Mueh, K. E.; Demmig-Adams, B.; Ebbert, V.; Turgeon, R.; Adams, W. W. Anatomical and photosynthetic acclimation to the light environment in species with differing mechanisms of phloem loading. *Proc. Natl. Acad. Sci. U. S. A.* **2005**, *102* (Track II), 12968–12973.

(80) Eichert, T.; Burkhardt, J. Quantification of stomatal uptake of ionic solutes using a new model system. *J. Exp. Bot.* **2001**, *52* (357), 771–781.

(81) Eichert, T.; Kurtz, A.; Steiner, U.; Goldbach, H. E. Size exclusion limits and lateral heterogeneity of the stomatal foliar uptake pathway for aqueous solutes and water-suspended nanoparticles. *Physiol. Plant.* **2008**, *134* (Schreiber 2005), 151–160.

(82) Gordon, K. C.; McGoverin, C. M. Raman mapping of pharmaceuticals. *Int. J. Pharm.* **2011**, *417* (1-2), 151–162.

(83) Fernández, V.; Eichert, T. Uptake of Hydrophilic Solutes Through Plant Leaves: Current State of Knowledge and Perspectives of Foliar Fertilization. *CRC. Crit. Rev. Plant Sci.* **2009**, *28* (1-2), 36–68.

(84) Nhan, L. Van; Ma, C.; Rui, Y.; Liu, S.; Li, X.; Xing, B.; Liu, L. Phytotoxic Mechanism of Nanoparticles: Destruction of Chloroplasts and Vascular Bundles and Alteration of Nutrient Absorption. *Sci. Rep.* **2015**, *5* (1), 11618.

(85) Zheng, L.; Hong, F.; Lu, S.; Liu, C. Effect of nano-TiO(2) on strength of naturally aged seeds and growth of spinach. *Biol. Trace Elem. Res.* **2005**, *104* (1), 83–92.

(86) Wijnhoven, S. W. P.; Peijnenburg, W. J. G. M.; Herberts, C. A.; Hagens, W. I.; Oomen, A. G.; Heugens, E. H. W.; Roszek, B.; Bisschops, J.; Gosens, I.; Van De Meent, D.; et al. Nano-silver – a review of available data and knowledge gaps in human and environmental risk assessment. *Nanotoxicology* **2009**, *3* (2), 109–138.

(87) Shi, J.; Peng, C.; Yang, Y.; Yang, J.; Zhang, H.; Yuan, X.; Chen, Y.; Hu, T. Phytotoxicity and accumulation of copper oxide nanoparticles to the Cu-tolerant plant Elsholtzia splendens. *Nanotoxicology* **2014**, *8* (2), 179–188.

(88) Tolaymat, T. M.; El Badawy, A. M.; Genaidy, A.; Scheckel, K. G.; Luxton, T. P.; Suidan, M. An evidence-based environmental perspective of manufactured silver nanoparticle in syntheses and applications: a systematic review and critical appraisal of peer-reviewed scientific papers. *Sci. Total Environ.* **2010**, *408* (5), 999–1006.

(89) Zhang, Z.; Guo, H.; Deng, Y.; Xing, B.; He, L. Mapping gold nanoparticles on and in edible leaves in situ using surface enhanced Raman spectroscopy. *RSC Adv.* **2016**, *6*, 1–22.

(90) Munro, C. H.; Smith, W. E.; Garner, M.; Clarkson, J.; White, P. C. Characterization of the surface of a citrate-reduced colloid optimized for use as a substrate for surface-enhanced resonance Raman scattering. *Langmuir* **1995**, *11* (10), 3712–3720.

(91) Zhang, Y.; Wang, F.; Yin, H.; Hong, M. Nonuniform Distribution of Capping Ligands Promoting Aggregation of Silver Nanoparticles for Use as a Substrate for SERS. *Adv. Nanoparticles* **2013**, *2013* (May), 104–111.

(92) Lau, B. L. T.; Hockaday, W. C.; Ikuma, K.; Furman, O.; Decho, A. W. A preliminary assessment of the interactions between the capping agents of silver nanoparticles and environmental organics. *Colloids Surfaces A Physicochem. Eng. Asp.* **2013**, *435*, 22–27.

(93) Yaffe, N. R.; Blanch, E. W. Effects and anomalies that can occur in SERS spectra of biological molecules when using a wide range of aggregating agents for hydroxylamine-reduced and citrate-reduced silver colloids. *Vib. Spectrosc.* **2008**, *48* (2), 196–201.

(94) Graff, M.; Bukowska, J. Adsorption of enantiomeric and racemic cysteine on a silver electrode - SERS sensitivity to chirality of adsorbed molecules. *J. Phys. Chem. B* **2005**, *109* (19), 9567–9574.

(95) Jing, C.; Fang, Y. Experimental (SERS) and theoretical (DFT) studies on the adsorption behaviors of L -cysteine on gold / silver nanoparticles. **2007**, *332*, 27–32.

(96) Gondikas, A. P.; Morris, A.; Reinsch, B. C.; Marinakos, S. M.; Lowry, G. V; Hsu-Kim, H. Cysteine-induced modifications of zero-valent silver nanomaterials: Implications for particle surface chemistry, aggregation, dissolution, and silver speciation. *Environ. Sci. Technol.* **2012**, *46*, 7037–7045.

(97) Espina Palanco, M.; Mogensen, K. B.; Kneipp, K. Raman spectroscopic probing of plant material using SERS. *J. Raman Spectrosc.* **2016**, *47* (2), 156–161.

(98) Ma, C.; Chhikara, S.; Minocha, R.; Long, S.; Musante, C.; White, J. C.; Xing, B.; Dhankher, O. P. Reduced Silver Nanoparticle Phytotoxicity in Crambe abyssinica with Enhanced Glutathione Production by Overexpressing Bacterial ??-Glutamylcysteine Synthase. *Environ. Sci. Technol.* **2015**, *49* (16), 10117–10126.

(99) Li, Y.; Dankher, O. P.; Carreira, L.; Smith, A. P.; Meagher, R. B. The shoot-specific expression of γ-glutamylcysteine synthetase directs the long-distance transport of thiol-peptides to roots conferring tolerance to mercury and arsenic. *Plant Physiol.* **2006**, *141* (1), 288–298.

(100) Stamplecoskie, K. G.; Scaiano, J. C.; Tiwari, V. S.; Anis, H. Optimal size of silver nanoparticles for surface-enhanced Raman spectroscopy. *J. Phys. Chem. C* **2011**, *115* (5), 1403–1409.

(101) Liu, Q.; Chen, B.; Wang, Q.; Shi, X.; Xiao, Z.; Lin, J.; Fang, X. Carbon nanotubes as molecular transporters for walled plant cells. *Nano Lett.* **2009**, *9* (3), 1007–1010.

(102) Deng, Y.; White, J. C.; Xing, B. Interactions between engineered nanomaterials and agricultural crops: implications for food safety. *J. Zhejiang Univ. Sci. A* **2014**, *15* (8), 552–572.

(103) Quadros, M. E.; Marr, L. C. Environmental and Human Health Risks of Aerosolized Silver Nanoparticles. *J. Air Waste Manage. Assoc.* **2010**, *60* (7), 770–781.

(104) Panyala, N. R.; Peña-Méndez, E. M.; Havel, J. Silver or silver nanoparticles: a hazardous threat to the environment and human health. *J Appl Biomed* **2008**, *6* (3), 117–129.

(105) AshaRani, P. V; Low Kah Mun, G.; Hande, M. P.; Valiyaveettil, S. Cytotoxicity and Genotoxicity of Silver Nanoparticles in Human Cells. *ACS Nano* **2009**, *3* (2), 279–290.

(106) Lu, W.; Senapati, D.; Wang, S.; Tovmachenko, O.; Singh, A. K.; Yu, H.; Ray, P. C. Effect of surface coating on the toxicity of silver nanomaterials on human skin keratinocytes. *Chem. Phys. Lett.* **2010**, *487* (1-3), 92–96.

(107) Suslow, T. *Postharvest chlorination: Basic properties and key points for effective disinfection*; University of California, Division of Agriculture and Natural Resources, 1997.

(108) Zhou, B.; Luo, Y.; Turner, E. R.; Wang, Q.; Schneider, K. R. Evaluation of Current Industry Practices for Maintaining Tomato Dump Tank Water Quality during Packinghouse Operations. *J. Food Process. Preserv.* **2014**, *38* (6), 2201–2208.

(109) Parish, M. E.; Beuchat, L. R.; Suslow, T. V; Harris, L. J.; Garrett, E. H.; Farber, J. N.; Busta, F. F. Methods to reduce/eliminate pathogens from fresh and fresh-cut produce. *Compr. Rev. food Sci. food Saf.* **2003**, *2* (s1), 161–173.

(110) Garrett, D. E. *Natural soda ash: occurrences, processing, and use*; Van Nostrand Reinhold, 1992.

(111) Zagory, D. Wash water sanitation: how do I compare different systems. In *16th Annual Post Harvest Conference & Trade Show, March*; 2000; pp 14–15.

(112) Barrera, M. J.; Blenkinsop, R.; Warriner, K. The effect of different processing parameters on the efficacy of commercial post-harvest washing of minimally processed spinach and shredded lettuce. *Food Control* **2012**, *25* (2), 745–751.

(113) Simons, L. K.; Sanguansri, P. Advances in the washing of minimally processed vegetables. *Food Aust. Off. J. CAFTA AIFST* **1997**.

(114) Baur, S.; Klaiber, R.; Hammes, W. P.; Carle, R. Sensory and microbiological quality of shredded, packaged iceberg lettuce as affected by pre-washing procedures with chlorinated and ozonated water. *Innov. Food Sci. Emerg. Technol.* **2004**, *5* (1), 45–55.

(115) Francis, G. A.; O'Beirne, D. Effects of vegetable type and antimicrobial dipping on survival and growth of Listeria innocua and E. coli. *Int. J. food Sci. Technol.* **2002**, *37* (6), 711–718.

(116) Watada, A. E.; Qi, L. Quality control of minimally-processed vegetables. In *International Symposium on Vegetable Quality of Fresh and Fermented Vegetables 483*; 1997; pp 209–220.

(117) Varoquaux, P.; Mazollier, J. Overview of the European fresh-cut produce industry. *Fresh-cut Fruits Veg. CRC Press. NY, USA* **2002**, 21–43.

(118) Yang, Y.; Wang, Y.; Zhang, X.; Qi, G.; Xu, S.; Xu, W. A facile method of removing several common surface-enhanced Raman scattering probe molecules adsorbed on Ag with sodium borohydride solution. *J. Opt.* **2015**, *17* (7), 75003.

(119) Michota, A.; Bukowska, J. Surface-enhanced Raman scattering (SERS) of 4-mercaptobenzoic acid on silver and gold substrates. *J. Raman Spectrosc.* **2003**, *34* (1), 21–25.

(120) Talley, C. E.; Jusinski, L.; Hollars, C. W.; Lane, S. M.; Huser, T. Intracellular pH sensors based on surface-enhanced raman scattering. *Anal. Chem.* **2004**, *76* (23), 7064–7068.

(121) Chen, J.; Li, Y.; Huang, K.; Wang, P.; He, L.; Carter, K. R.; Nugen, S. R. Nanoimprinted Patterned Pillar Substrates for Surface-Enhanced Raman Scattering Applications. *ACS Appl. Mater. Interfaces* **2015**, *7* (39), 22106–22113.

(122) Hunyadi, S. E.; Murphy, C. J. Bimetallic silver–gold nanowires: fabrication and use in surface-enhanced Raman scattering. *J. Mater. Chem.* **2006**, *16* (40), 3929–3935.

(123) Yan, J.; Han, X.; He, J.; Kang, L.; Zhang, B.; Du, Y.; Zhao, H.; Dong, C.; Wang, H.-L.; Xu, P. Highly sensitive surface-enhanced Raman spectroscopy (SERS) platforms based on silver nanostructures fabricated on polyaniline membrane surfaces. *ACS Appl. Mater. Interfaces* **2012**, *4* (5), 2752–2756.

(124) Amarjargal, A.; Tijing, L. D.; Shon, H. K.; Park, C.-H.; Kim, C. S. Facile in situ growth of highly monodispersed Ag nanoparticles on electrospun PU nanofiber membranes: Flexible and high efficiency substrates for surface enhanced Raman scattering. *Appl. Surf. Sci.* **2014**, *308*, 396–401.

(125) Tiwari, V. S.; Oleg, T.; Darbha, G. K.; Hardy, W.; Singh, J. P.; Ray, P. C. Non-resonance SERS effects of silver colloids with different shapes. *Chem. Phys. Lett.* **2007**, *446* (1-3), 77–82.

(126) Faulds, K.; Littleford, R. E.; Graham, D.; Dent, G.; Smith, W. E. Comparison of surface-enhanced resonance Raman scattering from unaggregated and aggregated nanoparticles. *Anal. Chem.* **2004**, *76* (3), 592–598.

(127) Bukhtiyarov, V. I.; Hävecker, M.; Kaichev, V. V; Knop-Gericke, A.; Mayer, R. W.; Schlögl, R. Atomic oxygen species on silver: Photoelectron spectroscopy and x-ray absorption studies. *Phys. Rev. B* **2003**, *67* (23), 235422.

(128) Bobrov, K.; Guillemot, L. Nanostructure formation by reactions of H 2 O with pre-adsorbed O on a Ag (110) surface. *Surf. Sci.* **2007**, *601* (15), 3268–3275.

(129) Guillemot, L.; Bobrov, K. On the formation of OH ordered layers by dissociation of H 2 O on an oxygen covered Ag (110) surface: An STM investigation. *Surf. Sci.* **2007**, *601* (3), 871–875.

(130) Ovissipour, M.; Sablani, S. S.; Rasco, B. Engineered nanoparticle adhesion and removal from tomato surfaces. *J. Agric. Food Chem.* **2013**, *61* (42), 10183–10190.

(131) Geranio, L.; Heuberger, M.; Nowack, B. The behavior of silver nanotextiles during washing. *Environ. Sci. Technol.* **2009**, *43* (21), 8113–8118.

(132) Graedel, T. E. Corrosion mechanisms for silver exposed to the atmosphere. *J. Electrochem. Soc.* **1992**, *139* (7), 1963–1970.

(133) Liang, A.; Zhang, N.; Jiang, Z.; Liu, R. Nanosilver resonance scattering spectral method for determination of hydroxyl radical and its application. *Sci. China Ser. B Chem.* **2008**, *51* (3), 226–232.

(134) Bodik, I.; Gašpariková, E.; Dančová, L.; Kalina, A.; Hutňan, M.; Drtil, M. Influence of disinfectants on domestic wastewater treatment plant performance. *Bioresour. Technol.* **2008**, *99* (3), 532–539.

(135) Impellitteri, C. A.; Tolaymat, T. M.; Scheckel, K. G. The Speciation of Silver Nanoparticles in Antimicrobial Fabric Before and After Exposure to a Hypochlorite/Detergent Solution. *J. Environ. Qual.* **2009**, *38* (4), 1528–1530.

(136) Choi, O.; Deng, K. K.; Kim, N. J.; Ross, L.; Surampalli, R. Y.; Hu, Z. The inhibitory effects of silver nanoparticles, silver ions, and silver chloride colloids on microbial growth. *Water Res.* **2008**, *42* (12), 3066–3074.

(137) Ratte, H. T. Bioaccumulation and toxicity of silver compounds: a review. *Environ. Toxicol. Chem.* **1999**, *18* (1), 89–108.

(138) Hadrup, N.; Lam, H. R. Oral toxicity of silver ions, silver nanoparticles and colloidal silver–a review. *Regul. Toxicol. Pharmacol.* **2014**, *68* (1), 1–7.

(139) Carlson, C.; Hussain, S. M.; Schrand, A. M.; K. Braydich-Stolle, L.; Hess, K. L.; Jones, R. L.; Schlager, J. J. Unique cellular interaction of silver nanoparticles: size-dependent generation of reactive oxygen species. *J. Phys. Chem. B* **2008**, *112* (43), 13608–13619.